



Turing–Hopf bifurcation in the predator–prey model with cross-diffusion considering two different prey behaviours’ transition

Yehu Lv 

Received: 4 June 2021 / Accepted: 8 November 2021 / Published online: 26 November 2021
© The Author(s), under exclusive licence to Springer Nature B.V. 2021

Abstract In this paper, we study the Turing–Hopf bifurcation in the predator–prey model with cross-diffusion considering the individual behaviour and herd behaviour transition of prey population subject to homogeneous Neumann boundary condition. Firstly, we study the non-negativity and boundedness of solutions corresponding to the temporal model, spatiotemporal model and the existence and priori boundedness of solutions corresponding to the spatiotemporal model without cross-diffusion. Then by analysing the eigenvalues of characteristic equation associated with the linearized system at the positive constant equilibrium point, we investigate the stability and instability of the corresponding spatiotemporal model. Moreover, by calculating and analysing the normal form on the centre manifold associated with the Turing–Hopf bifurcation, we investigate the dynamical classification near the Turing–Hopf bifurcation point in detail. At last, some numerical simulations results are given to support our analytic results.

Keywords Turing–Hopf bifurcation · Predator–prey model · Self-diffusion · Cross-diffusion · Individual behaviour · Herd behaviour · Spatially inhomogeneous periodic solution

Mathematics Subject Classification 35 Partial differential equations · 58 Global analysis, analysis on manifolds · 92 Biology and other natural sciences

1 Introduction

Since the groundbreaking works of Lotka [1] and Volterra [2], the predator–prey model is used to describe the dynamical interaction between two species and has been widely researched by many scholars in the fields of biology and mathematics [3,4]. It is well known that there are many functional response functions which are used to describe the interactional effect between the prey and predator species. For instance, the Holling I–III types [5,6], ratio-dependent type [7,8], Beddington–DeAngelis type [9], the different types with Allee effect [10–12] and so on.

Notice the fact that in natural ecosystem, many species may gather together and form herds to search for food resources or to defend the predators, which means that all members of a group do not interact at a time. This behaviour is often called as the herd behaviour. Recently, the authors in [13] have proposed a more realistic predator–prey model to describe this behaviour which can be written as

$$\begin{cases} \frac{du}{dt} = u(1-u) - \sqrt{u}v, \\ \frac{dv}{dt} = \tilde{\gamma}v(-\tilde{\beta} + \sqrt{u}), \end{cases} \quad (1)$$

Y. Lv (✉)
School of Mathematical Sciences, Beijing Normal
University, Beijing 100875, China
e-mail: mathyehul@163.com

where $u(t)$ and $v(t)$ stand for the prey and predator densities at time t , respectively. Furthermore, $\tilde{\beta}\tilde{\gamma}$ is the death rate of the predator in the absence of prey, and $\tilde{\gamma}$ is the conversion or consumption rate of prey to predator. The basic idea is that the prey population often gather together in huge herds with the strongest individuals on the border and the weakest will stay in the middle region of the enclosed region. Therefore, the prey which gathers together in the boundary region will be hunted by the predator. That is to say that, the prey population that occupies the outermost positions in the herds will be hunted by the predator.

In recent years, many predator–prey models with herd behaviour without diffusion term have been studied. Saha et al. [14] have studied a predator–prey model with herd behaviour and disease in prey incorporating prey refuge, which is an eco-epidemiological model of an infected predator–prey system. They assume that the susceptible prey shows the herd behaviour. The conditions for which the equilibrium point changes their stability and also the conditions for occurring Hopf bifurcation have been analysed. Manna et al. [15] have studied the dynamics of a predator–prey model with Allee effect and herd behaviour, where both predator and prey show herd behaviour. Here, the authors used the linear functional response function. A steady-state analysis has been performed, and some conditions for Hopf bifurcation are derived. Maiti et al. [16] have studied the dynamical behaviours of a predator–prey system with herd behaviour and the Holling type II functional response function, where both the predator and prey show herd behaviours. The positivity, boundedness and stability of equilibrium point are discussed.

From [17–20], we see that various reaction–diffusion predator–prey models have been extensively studied in the last decades. By considering the fact that in real natural environment, apart from the natural dispersive force of movement of an individual which is usually referred as the self-diffusion, there exists a mutual interference between individuals and is usually referred as the cross-diffusion, see [21–23] for details. Recently, cross-diffusion term has appeared in different fields, such as the population dynamics and ecology [24–27] and chemical reactions [28–31]. Furthermore, cross-diffusion is taken into consideration in predator–prey model which is used to measure the situation that the prey keeps away from the predator and conversely. Notice also that in recent years, many researchers have shifted from the study of the formation

of stationary spatial patterns induced by Turing instability to the study of the formation of spatiotemporal patterns. For example, by combining with the model (1) and considering the self-diffusion and cross-diffusion, Tang et al. [32] have proposed a predator–prey model with herd behaviour and cross-diffusion, and they study the spatiotemporal dynamics near Turing–Hopf bifurcation point of the proposed model. Faria [33] computed the normal forms on centre manifolds (or other invariant manifolds) for partial functional differential equations (PFDEs) near the positive constant equilibrium point. Especially, when a Hopf bifurcation occurs, Faria [33] used the obtained normal forms to study the qualitative behaviours of solutions on those manifolds. In [34], Song et al. have proposed a rigorous procedure for calculating the normal form for the codimension-two Turing–Hopf bifurcation in the general reaction–diffusion system and to investigate the dynamical classification near the Turing–Hopf bifurcation point in detail.

Notice the fact that if the herd is too small, it may not be possible for the herd to form an appropriate group defence. In other words, if the herd is too small, the boundary of the herd may consist of the total number of the population. Thus, De Assis et al. [35] have proposed a modified predator–prey model with herd behaviour by considering large prey populations which display herd behaviour, and small prey populations which display individual behaviour. From a mathematical point of view, the interaction term a_1uv can be used to describe a small number of prey populations, and $a_2\sqrt{uv}$ can be used to describe a large prey populations. Thus, the response function of their model is described by a piecewise function

$$g(u) = \begin{cases} a_1u, & \text{if } 0 \leq u \leq h_1, \\ a_2\sqrt{u}, & \text{if } u > h_1, \end{cases}$$

where h_1 represents a critical threshold of group size for effective defence. By considering that in real life, a smooth transition between ineffective and effective group defence is expected, at least for some species, and the function $g'(u)$ is discontinuous, the authors in [35] have proposed the following response function

$$f(u) = a \frac{u}{\sqrt{u} + h_2},$$

where a and h_2 are parameters for which the biological interpretation will be explained after some calculations. When $u \rightarrow 0$ and $u \rightarrow \infty$, the authors in [35] have

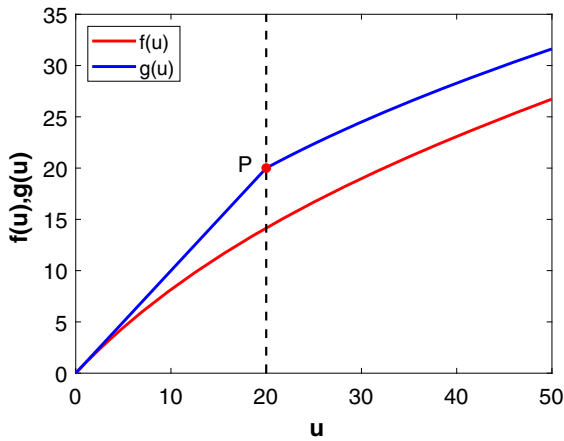


Fig. 1 The graphs of response functions $f(u)$ and $g(u)$ for $a_1 = 1$, $a_2 = \sqrt{20}$ and $h_1 = h_2 = \tilde{h} = 20$

created a smooth transition function $f(u)$ that approximates $g(u)$ by letting $g(u)/f(u)$ goes to one. Through simple calculations, the authors in [35] obtained that $a = a_2$ and $h_2 = (a_2/a_1)^2$. Furthermore, it follows that $h_1 = (a_2/a_1)^2$ from the continuity of $g(u)$, i.e. the critical threshold h_1 of group size for effective defence and the threshold h_2 is consistent. Thus, $f(u)$ can be seen as an approximation of $g(u)$ with a smooth transition for the individual behaviour a_1u and the group defence $a_2\sqrt{u}$. For convenience, the authors in [35] let $h_1 = h_2 = \tilde{h}$. Then, the functional response function of their proposed model can be written as

$$\tilde{f}(u, v) = a \frac{u}{\sqrt{u + \tilde{h}}} v.$$

Here, by setting $a_1 = 1$ and $a_2 = \sqrt{20}$, then $h_1 = h_2 = \tilde{h} = 20$, we plot the graphs of $f(u)$ and $g(u)$ in Fig. 1. The coordinate of point P is $(20, 20)$.

Thus, based on the above facts, the authors in [35] have proposed a modified predator–prey model with herd behaviour described by the following ordinary differential equations

$$\begin{cases} \frac{du}{dt} = ru \left(1 - \frac{u}{K}\right) - a \frac{u}{\sqrt{u + \tilde{h}}} v, \\ \frac{dv}{dt} = -mv + ea \frac{u}{\sqrt{u + \tilde{h}}} v, \end{cases} \quad (2)$$

where r is the intrinsic growth rates of the prey, K is the carrying capacity of the prey, a is the maximum value of prey consumed by per predator per unit time, \tilde{h} is a threshold for the transition between herd grouping and solitary behaviour, m is the death rate of the

predator in the absence of prey, and e is the conversion or consumption rate of prey to predator.

To the best of our knowledge, there are no results on spatiotemporal dynamics near Turing–Hopf bifurcation point of the model (2). Therefore, by assuming that the prey and predator populations are in an isolate patch and neglecting the impact of migration, including immigration and emigration, and introducing the spatial diffusion into the model (2), we consider the following modified predator–prey model with herd behaviour and cross-diffusion subject to homogeneous Neumann boundary condition for $x \in \Omega := (0, \ell\pi)$ with $\ell \in \mathbb{R}^+$. That is

$$\begin{cases} \frac{\partial u}{\partial t} = d_{11} \Delta u + d_{12} \Delta v + ru \left(1 - \frac{u}{K}\right) - a \frac{u}{\sqrt{u + \tilde{h}}} v, & x \in \Omega, t > 0, \\ \frac{\partial v}{\partial t} = d_{21} \Delta u + d_{22} \Delta v - mv + ea \frac{u}{\sqrt{u + \tilde{h}}} v, & x \in \Omega, t > 0, \\ \frac{\partial u}{\partial \mathbf{n}} = \frac{\partial v}{\partial \mathbf{n}} = 0, & x \in \partial\Omega, t > 0, \\ u(x, 0) = \phi(x) \geq 0, v(x, 0) = \psi(x) \geq 0, & x \in \Omega, \end{cases} \quad (3)$$

where $u(x, t)$ and $v(x, t)$ describe the prey and predator densities at the spatial location x and at time t , respectively, the nonnegative constants d_{11} and d_{22} are the self-diffusion coefficients of the prey and the predator, respectively, and the nonnegative constants d_{12} , d_{21} are the cross-diffusion coefficients, which describe the respective population fluxes of preys and predators resulting from the presence of the other species, respectively, $\Delta u = \partial^2 u / \partial x^2$, $\Delta v = \partial^2 v / \partial x^2$, and \mathbf{n} is the outward unit normal vector at the smooth boundary $\partial\Omega$. Moreover, $\phi(x)$ and $\psi(x)$ are the initial functions. Furthermore, it is necessary to assume that $d_{11}d_{22} > d_{12}d_{21}$, which indicates that the flux of the respective densities in the spatial domain depends more strongly on their own density than on the other [36]. Especially, we point out that the condition $d_{11}d_{22} > d_{12}d_{21}$ can also be obtained in Sect. 3 which is one of the necessary conditions for the occurrence of Turing instability for model (4).

In this paper, by calculating the normal form for the codimension-two Turing–Hopf bifurcation in the model (4), we investigate the dynamical classification near the Turing–Hopf bifurcation point. It is necessary to point out the fact that, although we use the method of computing normal form which presented in [34], since we choose d_{11} as the bifurcation parameter and

the existence of cross-diffusion, the procedure of computing B_{11} and B_{13} needs to be deduced again, see ‘‘Appendix’’ for details.

The remaining part of this article is organized as follows. In Sect. 2, we show the non-negativity and boundedness of solutions corresponding to the temporal model and the spatiotemporal model, respectively. Furthermore, the existence and priori boundedness of solutions corresponding to the spatiotemporal model without cross-diffusion are also researched. Section 3 is devoted to the stability analysis of the proposed spatiotemporal model, including the stability analysis for the case without self-diffusion and cross-diffusion and the stability analysis for the case with self-diffusion and cross-diffusion. Furthermore, we plot the bifurcation diagram for model (4) in $d_{11} - \delta$ plane which can be found in Sect. 3. In Sect. 4, we compute the normal form on the centre manifold for Turing–Hopf bifurcation corresponding to the model (4) by using the method in [34]. Some numerical simulations are given to support the theoretical results in Sect. 5. Finally, we conclude this paper in Sect. 6.

2 Non-negativity and boundedness of solutions corresponding to the temporal model

With a non-dimensionalized change of variables

$$u \rightarrow \frac{1}{K}u, \quad v \rightarrow \frac{1}{eK}v, \quad t \rightarrow mt,$$

and let

$$d_{11} = \frac{d_{11}}{m}, \quad d_{12} = \frac{d_{12}}{m}, \quad d_{21} = \frac{d_{21}}{m}, \quad d_{22} = \frac{d_{22}}{m},$$

$$\gamma = \frac{r}{m}, \quad \beta = \frac{ae\sqrt{K}}{m},$$

then model (3) becomes the following non-dimensionalized model

$$\begin{cases} \frac{\partial u}{\partial t} = d_{11}\Delta u + d_{12}\Delta v + \gamma u(1-u) - \frac{\beta uv}{\sqrt{u+h}}, & x \in \Omega, \quad t > 0, \\ \frac{\partial v}{\partial t} = d_{21}\Delta u + d_{22}\Delta v - v + \frac{\beta uv}{\sqrt{u+h}}, & x \in \Omega, \quad t > 0, \\ \frac{\partial u}{\partial \mathbf{n}} = \frac{\partial v}{\partial \mathbf{n}} = 0, & x \in \partial\Omega, \quad t > 0, \\ u(x, 0) = \phi(x) \geq 0, \quad v(x, 0) = \psi(x) \geq 0, & x \in \Omega, \end{cases} \tag{4}$$

where $h = \tilde{h}/K$ represents the critical threshold of group size for effective defence in non-dimensional scaling. Since we assumed that there is an observable group defence effect, it is reasonable to take $0 < \tilde{h} < K$, and hence $0 < h < 1$.

The temporal model associated with the model (4) is

$$\begin{cases} \frac{du(t)}{dt} = \gamma u(t)(1-u(t)) - \frac{\beta u(t)v(t)}{\sqrt{u(t)+h}}, & t > 0, \\ \frac{dv(t)}{dt} = -v(t) + \frac{\beta u(t)v(t)}{\sqrt{u(t)+h}}, & t > 0, \\ u(0) \geq 0, \quad v(0) \geq 0. \end{cases} \tag{5}$$

For the temporal model (5), we have the following results.

Theorem 1 *Suppose that $\gamma > 0$, $\beta > 0$, $0 < h < 1$ and consider the system given by (5) and its trajectories $u(t)$, $v(t)$; if the initial value $u(0) \geq 0$, $v(0) \geq 0$, then the solutions $u(t)$ and $v(t)$ are always non-negative. Furthermore, for any solution $(u(t), v(t))$ of system (5), we have*

$$\limsup_{t \rightarrow \infty} u(t) \leq \frac{(\gamma + 1)^2}{4\gamma}, \quad \limsup_{t \rightarrow \infty} v(t) \leq \frac{(\gamma + 1)^2}{4\gamma}.$$

Proof In fact, the system (5) is composed of the following three subsystems

$$\begin{cases} \frac{du(t)}{dt} = \gamma u(t)(1-u(t)) - \frac{\beta u(t)v(t)}{\sqrt{u(t)+h}}, & t > 0, \\ \frac{dv(t)}{dt} = -v(t) + \frac{\beta u(t)v(t)}{\sqrt{u(t)+h}}, & t > 0, \\ u(0) > 0, \quad v(0) > 0, \end{cases} \tag{6}$$

$$\begin{cases} u(t) = 0, & t > 0, \\ \frac{dv(t)}{dt} = -v(t), & t > 0, \\ u(0) = 0, \quad v(0) \geq 0 \end{cases} \tag{7}$$

and

$$\begin{cases} \frac{du(t)}{dt} = \gamma u(t)(1 - u(t)), & t > 0, \\ v(t) = 0, & t > 0, \\ u(0) \geq 0, v(0) = 0. \end{cases} \tag{8}$$

Since it is easy to verify that the solution of (7) will approach the origin (0, 0) along the v -axis as $t \rightarrow \infty$ and the solution of (refh8) will tend to (1, 0) along the u -axis as $t \rightarrow \infty$, we only need to consider the solutions of (6). Assume $X(t) = (u(t), v(t))$ is a solution of system (6). If it does not remain in the first quadrant, then the solution either hits the u -axis or the v -axis in finite time. Thus, by combining with the analysis results of the subsystems (7) and (refh8), we can obtain that any solution $(u(t), v(t))$ of system (6) with non-negative initial value $(u(0), v(0))$ will remain positive for all $t > 0$, or will approach either the original or (1, 0) along the axes.

Next, the boundedness of solutions is confirmed. Let $\tilde{w}(t) = u(t) + v(t)$, then by adding

$$\frac{du(t)}{dt} = \gamma u(t)(1 - u(t)) - \frac{\beta u(t)v(t)}{\sqrt{u(t) + h}}$$

to

$$\frac{dv(t)}{dt} = -v(t) + \frac{\beta u(t)v(t)}{\sqrt{u(t) + h}},$$

we have

$$\begin{aligned} \frac{d\tilde{w}(t)}{dt} &= \gamma u(t)(1 - u(t)) + u(t) - \tilde{w}(t) \\ &\leq \frac{(\gamma + 1)^2}{4\gamma} - \tilde{w}(t) \end{aligned}$$

resulting in

$$\limsup_{t \rightarrow \infty} \tilde{w}(t) \leq \frac{(\gamma + 1)^2}{4\gamma}.$$

Furthermore, notice that $\tilde{w}(t) = u(t) + v(t)$, then we have

$$\begin{aligned} \limsup_{t \rightarrow \infty} u(t) &\leq \frac{(\gamma + 1)^2}{4\gamma}, \quad \limsup_{t \rightarrow \infty} v(t) \\ &\leq \frac{(\gamma + 1)^2}{4\gamma}. \end{aligned}$$

This concludes the proof. □

2.1 Non-negativity and boundedness of solutions corresponding to the spatiotemporal model

Theorem 2 *Suppose that $\gamma > 0$, $\beta > 0$, $0 < h < 1$ and $\Omega \subset \mathbb{R}$ is a bounded domain with smooth bound-*

ary. Then for any solution $(u(x, t), v(x, t))$ of model (4), we have

$$\begin{aligned} \limsup_{t \rightarrow \infty} \int_{\Omega} u(x, t) dx &\leq \frac{(\gamma + 1)^2}{4\gamma} |\Omega|, \\ \limsup_{t \rightarrow \infty} \int_{\Omega} v(x, t) dx &\leq \frac{(\gamma + 1)^2}{4\gamma} |\Omega|, \end{aligned}$$

where $|\Omega|$ is the length of the bounded domain Ω .

Proof Denote

$$M_1(t) = \int_{\Omega} u(x, t) dx, \quad M_2(t) = \int_{\Omega} v(x, t) dx,$$

then by integrating on both sides of each equation on the region Ω in system (4), we have

$$\begin{aligned} \frac{dM_1(t)}{dt} &= \int_{\Omega} (d_{11} \Delta u + d_{12} \Delta v) dx \\ &\quad + \int_{\Omega} (\gamma u(1 - u) - \frac{\beta uv}{\sqrt{u + h}}) dx, \\ \frac{dM_2(t)}{dt} &= \int_{\Omega} (d_{21} \Delta u + d_{22} \Delta v) dx \\ &\quad + \int_{\Omega} (-v + \frac{\beta uv}{\sqrt{u + h}}) dx. \end{aligned} \tag{9}$$

Let $M(t) = M_1(t) + M_2(t)$, then by combining with Eq. (9) and noticing the homogeneous Neumann boundary defined in system (4), we can obtain

$$\begin{aligned} \frac{dM(t)}{dt} &= \frac{dM_1(t)}{dt} + \frac{dM_2(t)}{dt} \\ &= \int_{\Omega} (\gamma u(1 - u) - v) dx \\ &= \int_{\Omega} (\gamma u(1 - u) + u) dx - M(t) \\ &\leq \frac{(\gamma + 1)^2}{4\gamma} |\Omega| - M(t), \end{aligned}$$

from which we obtain that

$$\limsup_{t \rightarrow \infty} M(t) \leq \frac{(\gamma + 1)^2}{4\gamma} |\Omega|.$$

Furthermore, notice that $M(t) = M_1(t) + M_2(t)$, then we have

$$\begin{aligned} \limsup_{t \rightarrow \infty} \int_{\Omega} u(x, t) dx &\leq \frac{(\gamma + 1)^2}{4\gamma} |\Omega|, \\ \limsup_{t \rightarrow \infty} \int_{\Omega} v(x, t) dx &\leq \frac{(\gamma + 1)^2}{4\gamma} |\Omega|. \end{aligned}$$

This proof is completed. □

2.2 The existence and priori boundedness of solutions corresponding to the spatiotemporal model without cross-diffusion

In this section, we give out a sufficient condition for the existence of a positive solution of system (4) without cross-diffusion. Meanwhile, we derive a priori boundedness of the solution. When $d_{12} = d_{21} = 0$, system (4) becomes

$$\begin{cases} \frac{\partial u}{\partial t} = d_{11}\Delta u + \gamma u(1-u) - \frac{\beta uv}{\sqrt{u+h}}, & x \in \Omega, t > 0, \\ \frac{\partial v}{\partial t} = d_{22}\Delta v - v + \frac{\beta uv}{\sqrt{u+h}}, & x \in \Omega, t > 0, \\ \frac{\partial u}{\partial \mathbf{n}} = \frac{\partial v}{\partial \mathbf{n}} = 0, & x \in \partial\Omega, t > 0, \\ u(x, 0) = \phi(x) \geq 0, v(x, 0) = \psi(x) \geq 0, & x \in \Omega. \end{cases} \tag{10}$$

Theorem 3 Suppose that $\gamma > 0, \beta > 0, 0 < h < 1$ and $\Omega \subset \mathbb{R}^n$ is a bounded domain with smooth boundary. Then we have the following results:

- (i) For $\phi(x) \geq 0, \psi(x) \geq 0$ and $\phi(x) \not\equiv 0, \psi(x) \not\equiv 0$, system (10) has a unique solution $(u(x, t), v(x, t))$ satisfying $0 < u(x, t) \leq u^*(t), 0 < v(x, t) \leq v^*(t)$ for $t > 0$ and $x \in \Omega$, where $(u^*(t), v^*(t))$ is the unique solution of

$$\begin{cases} \frac{du}{dt} = \gamma u(1-u), & t > 0, \\ \frac{dv}{dt} = -v + \frac{\beta uv}{\sqrt{u+h}}, & t > 0, \\ u(0) = \phi^* = \sup_{x \in \bar{\Omega}} \phi(x), v(0) = \psi^* = \sup_{x \in \bar{\Omega}} \psi(x), \end{cases}$$

and $\bar{\Omega}$ represents the closure of Ω ;

- (ii) For any solution $(u(x, t), v(x, t))$ of system (10), we have

$$\limsup_{t \rightarrow \infty} u(x, t) \leq 1, \quad \limsup_{t \rightarrow \infty} \int_{\Omega} v(x, t) dx \leq (\gamma + 1)|\Omega|.$$

Proof Denote

$$f(u, v) = \gamma u(1-u) - \frac{\beta uv}{\sqrt{u+h}},$$

$$g(u, v) = -v + \frac{\beta uv}{\sqrt{u+h}},$$

then we have $f_v \leq 0$ and $g_u \geq 0$ for $(u, v) \in \mathbb{R}_+^2 = \{(u, v) \mid u \geq 0, v \geq 0\}$. Thus, the system (10) is a mixed quasi-monotone system.

Furthermore, if we assume that $(u_1(x, t), v_1(x, t)) = (0, 0)$ and $(u_2(x, t), v_2(x, t)) = (u^*(t), v^*(t))$, then we can obtain

$$\begin{aligned} & \frac{\partial u_2}{\partial t} - d_{11}\Delta u_2 - f(u_2, v_1) \\ & = 0 \geq 0 \\ & = \frac{\partial u_1}{\partial t} - d_{11}\Delta u_1 - f(u_1, v_2), \\ & \frac{\partial v_2}{\partial t} - d_{22}\Delta v_2 - g(u_2, v_2) \\ & = 0 \geq 0 \\ & = \frac{\partial v_1}{\partial t} - d_{11}\Delta v_1 - g(u_1, v_1), \end{aligned}$$

and $0 \leq \phi(x) \leq \phi^*, 0 \leq \psi(x) \leq \psi^*$, so $(u_1(x, t), v_1(x, t))$ and $(u_2(x, t), v_2(x, t))$ are the lower and upper solutions of system (10), respectively.

According to Theorem 3.3 in Section 8.3 of Chapter 8 in [37], we know that (10) has a unique globally defined solution $(u(x, t), v(x, t))$ which satisfies

$$0 \leq u(x, t) \leq u^*(t), \quad 0 \leq v(x, t) \leq v^*(t), \quad t > 0.$$

The strong maximum principle implies that $u(x, t) > 0, v(x, t) > 0$ when $t > 0$, for $x \in \Omega$. This completes the proof of conclusion (i).

From the above discussion, we can obtain that $0 < u(x, t) \leq u^*(t), 0 < v(x, t) \leq v^*(t)$ for all $t > 0$, and $u^*(t)$ is the unique solution of

$$\frac{du}{dt} = \gamma u(1-u), \quad u(0) = \phi^* > 0.$$

One can see that $u^*(t) \rightarrow 1$ as $t \rightarrow \infty$. Thus, for any $\varepsilon > 0$, there exists $t_0 > 0$ such that $u(x, t) \leq 1 + \varepsilon$ for $t > t_0$ and $x \in \bar{\Omega}$, which implies that $\limsup_{t \rightarrow \infty} \sup_{x \in \bar{\Omega}} u(x, t) \leq 1$.

Furthermore, if let

$$N_1(t) = \int_{\Omega} u(x, t) dx, \quad N_2(t) = \int_{\Omega} v(x, t) dx,$$

$$N(t) = N_1(t) + N_2(t),$$

then

$$\frac{dN_1(t)}{dt} = \int_{\Omega} d_{11}\Delta u dx + \int_{\Omega} \left(\gamma u(1-u) - \frac{\beta uv}{\sqrt{u+h}} \right) dx,$$

$$\frac{dN_2(t)}{dt} = \int_{\Omega} d_{22}\Delta v dx + \int_{\Omega} \left(-v + \frac{\beta uv}{\sqrt{u+h}} \right) dx.$$

By using the homogeneous Neumann boundary condition, we can obtain

$$\begin{aligned} \frac{dN(t)}{dt} &= \frac{dN_1(t)}{dt} + \frac{dN_2(t)}{dt} \\ &= -N_2(t) + \gamma \int_{\Omega} u(1-u)dx \\ &= \gamma \int_{\Omega} u(1-u)dx - (N_1(t) + N_2(t)) + N_1(t) \\ &= \gamma \int_{\Omega} u(1-u)dx - (N_1(t) + N_2(t)) + \int_{\Omega} u(x,t)dx \\ &\leq -N(t) + (\gamma + 1)N_1(t). \end{aligned}$$

From $\lim_{t_0 \rightarrow \infty} \sup_{t > t_0} u(x,t) \leq 1$, we can obtain that $\lim_{t_0 \rightarrow \infty} \sup_{t > t_0} N_1(t) \leq |\Omega|$. Thus for small $\varepsilon > 0$, there exists $t_1 \geq 0$ such that

$$\frac{dN(t)}{dt} \leq -N(t) + (\gamma + 1)|\Omega|, \quad t > t_1. \tag{11}$$

It is well known that the solution $N(t)$ of

$$\frac{dN(t)}{dt} = -N(t) + (\gamma + 1)(1 + \varepsilon)|\Omega|$$

satisfies

$$\lim_{t \rightarrow \infty} N(t) = (\gamma + 1)(1 + \varepsilon)|\Omega|.$$

In terms of comparison principle and using (11) we obtain that, for $t_2 > t_1$

$$\int_{\Omega} v(x,t)dx = N_2(t) < N(t) \leq (\gamma + 1)(1 + \varepsilon)|\Omega| + \varepsilon, \quad t > t_2,$$

which implies that

$$\lim_{t_2 \rightarrow \infty} \sup_{t > t_2} \int_{\Omega} v(x,t)dx \leq (\gamma + 1)|\Omega|.$$

This completes the proof of conclusion (ii). □

3 Stability analysis of the corresponding spatiotemporal model

The system (4) has two boundary equilibrium points $(0, 0)$ and $(1, 0)$. Moreover, when $0 < \delta < (1/\sqrt{h+1})$, the system (4) has a unique positive constant equilibrium point $E_*(u_*, v_*)$ with

$$u_* = \frac{\delta}{2} \left(\delta + \sqrt{\delta^2 + 4h} \right), \quad v_* = \gamma u_*(1 - u_*),$$

where $\delta = 1/\beta$ with $\beta > 0$, and $0 < h < 1, \gamma > 0$.

Defining a real-valued Hilbert space

$$\begin{aligned} \mathcal{X} := & \left\{ (u, v)^T \in H^2(0, \ell\pi) \times H^2(0, \ell\pi) : \frac{\partial u}{\partial x} \right. \\ & \left. = \frac{\partial v}{\partial x} = 0 \text{ at } x = 0, \ell\pi \right\} \end{aligned}$$

with the inner product defined by

$$[U_1, U_2] = \int_0^{\ell\pi} U_1^T U_2 \, dx$$

for $U_1 = (u_1, v_1)^T \in \mathcal{X}$ and $U_2 = (u_2, v_2)^T \in \mathcal{X}$. The linearization of system (4) at positive constant equilibrium point $E_*(u_*, v_*)$ is

$$\frac{d}{dt} \begin{pmatrix} u \\ v \end{pmatrix} = d\Delta \begin{pmatrix} u \\ v \end{pmatrix} + A \begin{pmatrix} u \\ v \end{pmatrix} \tag{12}$$

with

$$\begin{aligned} d\Delta &= \begin{pmatrix} d_{11} \frac{\partial^2}{\partial x^2} & d_{12} \frac{\partial^2}{\partial x^2} \\ d_{21} \frac{\partial^2}{\partial x^2} & d_{22} \frac{\partial^2}{\partial x^2} \end{pmatrix}, \\ A &= \begin{pmatrix} a_{11} & a_{12} \\ a_{21} & a_{22} \end{pmatrix} = \begin{pmatrix} \frac{\gamma u_*}{2(u_*+h)} (-3u_* + 1 - 2h) & -1 \\ \frac{\gamma(1-u_*)(u_*+2h)}{2(u_*+h)} & 0 \end{pmatrix} \\ &= \begin{pmatrix} \frac{\gamma(\delta^2(-3\delta^2-8h+1)+\delta\sqrt{\delta^2+4h}(-3\delta^2-2h+1))}{2\delta\sqrt{\delta^2+4h}+2\delta^2+4h} & -1 \\ \frac{\gamma(\delta\sqrt{\delta^2+4h}(2-2\delta^2-4h)+\delta^2(2-2\delta^2-8h)+8h)}{4(\delta\sqrt{\delta^2+4h}+\delta^2+2h)} & 0 \end{pmatrix}. \end{aligned} \tag{13}$$

It is well known that the eigenvalue problem

$$\begin{cases} \varphi''(x) = \tilde{\lambda}\varphi(x), & x \in (0, \ell\pi), \\ \varphi'(0) = \varphi'(\ell\pi) = 0 \end{cases}$$

has eigenvalues $\tilde{\lambda}_k = -k^2/\ell^2$ with corresponding normalized eigenfunctions

$$\gamma_k(x) = \frac{\cos(\frac{kx}{\ell})}{\|\cos(\frac{kx}{\ell})\|_{L^2}} = \begin{cases} \frac{1}{\sqrt{\ell\pi}}, & k = 0, \\ \frac{\sqrt{2}}{\sqrt{\ell\pi}} \cos(\frac{kx}{\ell}), & k \geq 1, \end{cases} \tag{14}$$

where $k \in \mathbb{N}_0 = \mathbb{N} \cup \{0\}$ is often called wave number, and $\mathbb{N}_0 = \mathbb{N} \cup \{0\}$ is the set of all non-negative integers, $\mathbb{N} = \{1, 2, \dots\}$ represents the set of all positive integers. Thus, the eigenfunctions of $d\Delta$ on \mathcal{X} corresponding to its eigenvalues have the form

$$\beta_k(x) = \begin{pmatrix} a_k \\ b_k \end{pmatrix} \gamma_k(x),$$

where $a_k, b_k \in \mathbb{R}$ and $\gamma_k(x)$ is defined by Eq. (14).

Let

$$\begin{pmatrix} y_1 \\ y_2 \end{pmatrix} = \sum_{k=0}^{\infty} \begin{pmatrix} a_k \\ b_k \end{pmatrix} \gamma_k(x)$$

be an eigenfunction of $d\Delta + A$ corresponding to an eigenvalue λ , that is

$$(d\Delta + A)(y_1, y_2)^T = \lambda(y_1, y_2)^T.$$

Then, we have

$$\mathcal{L}_k \begin{pmatrix} a_k \\ b_k \end{pmatrix} = \lambda \begin{pmatrix} a_k \\ b_k \end{pmatrix}, \quad k \in \mathbb{N}_0 = \mathbb{N} \cup \{0\},$$

where

$$\mathcal{L}_k = \begin{pmatrix} a_{11} - d_{11} \frac{k^2}{\ell^2} & a_{12} - d_{12} \frac{k^2}{\ell^2} \\ a_{21} - d_{21} \frac{k^2}{\ell^2} & a_{22} - d_{22} \frac{k^2}{\ell^2} \end{pmatrix}$$

which follows that the eigenvalues of $d\Delta + A$ are given by the eigenvalues of \mathcal{L}_k with $k \in \mathbb{N}_0 = \mathbb{N} \cup \{0\}$. Notice that the solutions of Eq. (12) can be obtained by using the eigenvalues and eigenvectors of the matrix $d\Delta + A$. Then by the Fourier expansion

$$\begin{pmatrix} u \\ v \end{pmatrix} = \sum_{k=0}^{\infty} q_k^T \begin{pmatrix} \xi_k^1 \\ \xi_k^2 \end{pmatrix} e^{\lambda t}, \quad q_k = \begin{pmatrix} q_{k1} \\ q_{k2} \end{pmatrix} \in \mathbb{C}^2, \tag{15}$$

which can be seen as a nontrivial solutions of Eq. (12), where

$$\xi_k^1(x) = \begin{pmatrix} \gamma_k(x) \\ 0 \end{pmatrix}, \quad \xi_k^2(x) = \begin{pmatrix} 0 \\ \gamma_k(x) \end{pmatrix}, \quad k \in \mathbb{N}_0 = \mathbb{N} \cup \{0\},$$

and by substituting (15) into (12), we can obtain the following sequence of characteristic equations Δ_k , i.e.

$$\lambda^2 - T_k \lambda + D_k = 0, \tag{16}$$

where

$$\begin{aligned} T_k &= a_{11} - (d_{11} + d_{22}) \frac{k^2}{\ell^2}, \\ D_k &= (d_{11}d_{22} - d_{12}d_{21}) \frac{k^4}{\ell^4} \\ &\quad - (a_{11}d_{22} + d_{21} - d_{12}a_{21}) \frac{k^2}{\ell^2} + a_{21}. \end{aligned} \tag{17}$$

By combining with Eqs. (16) and (17), and noticing that the necessary condition for the occurrence of Turing instability is $d_{11}d_{22} - d_{12}d_{21} > 0$ and

$$4(d_{11}d_{22} - d_{12}d_{21})a_{21} - (a_{11}d_{22} + d_{21} - d_{12}a_{21})^2 < 0,$$

then in the $d_{11} - \delta$ plane, we can define a curve \mathbf{L} by

$$\mathbf{L} : (a_{11}d_{22} + d_{21} - d_{12}a_{21}) - 2\sqrt{(d_{11}d_{22} - d_{12}d_{21})a_{21}} = 0. \tag{18}$$

According to [32], we know that if there exist a non-negative integer k_1 and a positive integer $k_2 \neq k_1$ such that $\Delta_{k_1} = 0$ has a pair of purely imaginary roots and $\Delta_{k_2} = 0$ has a simple zero root, and no other roots of (16) has a zero real part, and the corresponding transversality conditions hold, then we call the bifurcation in this case as a Turing–Hopf bifurcation.

3.1 Stability analysis for the case without self-diffusion and cross-diffusion

In the case of without self-diffusion or cross-diffusion ($d_{11} = d_{12} = d_{21} = d_{22} = 0$), the original system (4) becomes the following ordinary differential equation

$$\begin{cases} \frac{du}{dt} = \gamma u(1 - u) - \frac{\beta uv}{\sqrt{u+h}}, & t > 0, \\ \frac{dv}{dt} = -v + \frac{\beta uv}{\sqrt{u+h}}, & t > 0, \\ u(0) = u_0 \geq 0, \quad v(0) = v_0 \geq 0. \end{cases} \tag{19}$$

Clearly, the original system (4) and (19) have the same positive constant equilibrium point $E_*(u_*, v_*)$. By a simple linear analysis, we can obtain the following result.

Theorem 4 *For the positive constant equilibrium point $E_*(u_*, v_*)$ of system (19) with $\gamma > 0$, $\beta > 0$, $0 < h < 1$, we have the following results on its stability.*

- (i) *When $1/2 < h < 1$, the positive constant equilibrium point $E_*(u_*, v_*)$ is always asymptotically stable;*
- (ii) *When $0 < h \leq 1/2$, the positive constant equilibrium point $E_*(u_*, v_*)$ is asymptotically stable for*

$$\max\{0, \delta^*\} < \delta < \frac{1}{\sqrt{h+1}}, \quad \delta^* = \frac{1-2h}{\sqrt{3(1+h)}},$$

and unstable for $0 < \delta < \delta^$.*

Moreover, $\Delta_0 = 0$ has a pair of purely imaginary roots $\pm i\sqrt{D_0}$ iff $\delta = \delta^*$, which implies that system (19) undergoes a Hopf bifurcation at $\delta = \delta^*$ near the positive constant equilibrium point $E_*(u_*, v_*)$, and the Hopf bifurcation curve is defined by

$$\mathbf{H}_0 : \delta = \delta^* = \frac{1-2h}{\sqrt{3(1+h)}}. \tag{20}$$

Proof By combining with Eqs. (16), (17) and $0 < \delta < 1/\sqrt{h+1}$, we have

$$T_0 = a_{11}, \quad D_0 = a_{21} > 0.$$

Indeed, if $0 < \delta < 1/\sqrt{h+1}$, follows that $D_0 = a_{21} > 0$, then for the stability analysis of $E_*(u_*, v_*)$, it is sufficient to study the sign of

$$T_0 = a_{11} = \frac{\gamma u_*}{2(u_* + h)} (-3u_* + 1 - 2h).$$

Let $P(\delta) := -3u_* + 1 - 2h$, then by combining with

$$u_* = \frac{\delta}{2} \left(\delta + \sqrt{\delta^2 + 4h} \right),$$

we can obtain

$$P(\delta) = -\frac{3\delta}{2} \left(\delta + \sqrt{\delta^2 + 4h} \right) + 1 - 2h.$$

Notice that for $1/2 < h < 1$, $P(\delta)$ is always negative. For $0 < h \leq 1/2$, notice that $P(\delta)$ is decreasing with respect to δ , so the sign of $P(\delta)$ is determined by its root δ^* . Thus, $T_0 = a_{11}$ is positive for $\delta < \delta^*$ and negative conversely. Notice also that when $\delta = \delta^*$, we can obtain $T_0 = a_{11} = 0$. Thus, when $\delta = \delta^*$, by combining with $\lambda^2 - T_0\lambda + D_0 = 0$, we have $\lambda = \pm i\sqrt{D_0}$ iff $\delta = \delta^*$.

This completes the proof. □

3.2 Stability analysis for the case with self-diffusion and cross-diffusion

In this section, we investigate the effect of cross-diffusion on the positive constant equilibrium point $E_*(u_*, v_*)$ of the original system (4). We have the following Theorem 5.

Theorem 5 Assume that $\gamma > 0$, $\beta > 0$, $0 < h < 1$, \mathbf{H}_0 is defined by $\delta = \delta^* = (1 - 2h)/\sqrt{3(1 + h)}$ and \mathbf{L}_k is defined by

$$(d_{11}d_{22} - d_{12}d_{21}) \frac{k^4}{\ell^4} - (a_{11}d_{22} + d_{21} - d_{12}a_{21}) \frac{k^2}{\ell^2} + a_{21} = 0. \tag{21}$$

Then

(I) if $0 < d_{21} < (\ell^2\gamma(4h + 1))/3$, then original system (4) is always stable over the Hopf bifurcation curve \mathbf{H}_0 , that is, system (4) doesn't undergo Turing–Hopf bifurcation;

(II) if $(\ell^2\gamma(4h + 1))/3 < d_{21} < (d_{11}d_{22})/d_{12}$, then

(i) The Hopf bifurcation curve \mathbf{H}_0 intersects with the Turing bifurcation curve \mathbf{L}_k , and a codimension-2 Turing–Hopf bifurcation occurs at the intersect point (d_{11}^*, δ^*) , where

$$d_{11}^* = \frac{d_{12}d_{21} \frac{k_*^4}{\ell^4} + (d_{21} - d_{12} \frac{\gamma(4h+1)}{3}) \frac{k_*^2}{\ell^2} - \frac{\gamma(4h+1)}{3}}{d_{22} \frac{k_*^4}{\ell^4}},$$

$$\delta^* = \frac{1 - 2h}{\sqrt{3(1 + h)}};$$

(ii) For $(d_{11}, \delta) = (d_{11}^*, \delta^*)$, the equation $\Delta_0 = 0$ has a pair of purely imaginary roots $\pm i\omega_c$ and $\Delta_{k_*} = 0$ has a simple zero root, and for the system (4), there are no other roots with zero real parts, where

$$\omega_c = \sqrt{a_{21}(\delta^*)} = \sqrt{\frac{\gamma(4h + 1)}{3}}.$$

Proof The Turing bifurcation curve \mathbf{L}_k defined by (21) is followed from $D_k = 0$, i.e.

$$(d_{11}d_{22} - d_{12}d_{21}) \frac{k^4}{\ell^4} - (a_{11}d_{22} + d_{21} - d_{12}a_{21}) \frac{k^2}{\ell^2} + a_{21} = 0.$$

By combining with Eqs. (16) and (17), we can see that $T_k < 0$ provided that $a_{11} < 0$, and that $D_k > 0$ is equivalent to

$$d_{11} > \frac{d_{12}d_{21} \frac{k^4}{\ell^4} + (a_{11}d_{22} + d_{21} - d_{12}a_{21}) \frac{k^2}{\ell^2} - a_{21}}{d_{22} \frac{k^4}{\ell^4}}.$$

Notice that $a_{11}(\delta^*) = 0$, $a_{21}(\delta^*) = \gamma(4h + 1)/3$, and when

$$d_{12}d_{21} \frac{k^4}{\ell^4} + (a_{11}(\delta^*)d_{22} + d_{21} - d_{12}a_{21}(\delta^*)) \frac{k^2}{\ell^2} - a_{21}(\delta^*) < 0,$$

i.e. $0 < d_{21} < (\ell^2\gamma(4h + 1))/3$, the Turing bifurcation curve \mathbf{L}_k doesn't interact with the Hopf bifurcation curve \mathbf{H}_0 . Here, $a_{11}(\delta^*)$, $a_{21}(\delta^*)$ indicating a_{11} and a_{21} are dependent on δ^* , respectively. That is, system (4) is always asymptotically stable over the Hopf bifurcation curve \mathbf{H}_0 . Thus, the conclusion (I) is confirmed.

When $d_{11}d_{22} - d_{12}d_{21} > 0$ and

$$d_{12}d_{21} \frac{k^4}{\ell^4} + (a_{11}(\delta^*)d_{22} + d_{21} - d_{12}a_{21}(\delta^*)) \frac{k^2}{\ell^2} - a_{21}(\delta^*) > 0,$$

i.e. $(\ell^2\gamma(4h + 1))/3 < d_{21} < (d_{11}d_{22})/d_{12}$, the Turing bifurcation curve \mathbf{L}_k interact with the Hopf bifurcation curve \mathbf{H}_0 , then by substituting $\delta = \delta^*$ into $D_k = 0$ and solving $D_k = 0$ for d_{11} , we have that

$$d_{11}(k) = \frac{d_{12}d_{21} \frac{k^4}{\ell^4} + (d_{21} - d_{12} \frac{\gamma(4h+1)}{3}) \frac{k^2}{\ell^2} - \frac{\gamma(4h+1)}{3}}{d_{22} \frac{k^4}{\ell^4}}, \quad k > k^*,$$

where k^* is defined by Eq. (22). Furthermore, the symbol $[\cdot]$ in Eq. (22) stands for the integer part function.

$$k^* = \left[\ell \sqrt{\frac{(d_{12} \frac{\gamma(4h+1)}{3} - d_{21}) + \sqrt{(d_{21} - d_{12} \frac{\gamma(4h+1)}{3})^2 + \frac{4\gamma(4h+1)}{3} d_{12} d_{21}}}{2d_{12} d_{21}}} \right]. \tag{22}$$

Let

$$f(x) = \frac{d_{12} d_{21} x^2 + (d_{21} - d_{12} \frac{\gamma(4h+1)}{3})x - \frac{\gamma(4h+1)}{3}}{d_{22} x^2}, \quad x > k^*,$$

we can obtain that

$$f'(x) = \frac{(d_{12} \frac{\gamma(4h+1)}{3} - d_{21})x^2 + \frac{2\gamma(4h+1)}{3}x}{d_{22} x^4}, \quad x > k^*.$$

Therefore, if $(d_{12}\gamma(4h + 1))/3 - d_{21} < 0$, we have $f'(x) \geq 0$ for $x \leq x^*$, and $f'(x) < 0$ for $x > x^*$, where

$$x^* = \frac{2\gamma(4h + 1)}{3d_{21} - \gamma d_{12}(4h + 1)}.$$

By setting

$$k_* = \begin{cases} [\ell\sqrt{x^*}], & \text{if } d_{11}([\ell\sqrt{x^*}] + 1) \leq d_{11}([\ell\sqrt{x^*}]), \\ & x^* > k^*, \\ [\ell\sqrt{x^*}] + 1, & \text{if } d_{11}([\ell\sqrt{x^*}]) < d_{11}([\ell\sqrt{x^*}] + 1), \\ & x^* > k^*, \end{cases} \tag{23}$$

then there exists a $k_* > k^*$ such that $d_{11}^* = d_{11}(k_*) = \max_{k > k^*} d_{11}(k)$.

Furthermore, if $(d_{12}\gamma(4h + 1))/3 - d_{21} > 0$, we have $f'(x) \leq 0$ for $x \leq x^*$, and $f'(x) > 0$ for $x > x^*$. By setting

$$k_* = \begin{cases} [\ell\sqrt{x^*}] + 1, & \text{if } d_{11}([\ell\sqrt{x^*}] + 1) \leq d_{11}([\ell\sqrt{x^*}]), \\ & x^* > k^*, \\ [\ell\sqrt{x^*}], & \text{if } d_{11}([\ell\sqrt{x^*}]) < d_{11}([\ell\sqrt{x^*}] + 1), \\ & x^* > k^*, \end{cases}$$

then there exists a $k_* > k^*$ such that $d_{11}^* = d_{11}(k_*) = \min_{k > k^*} d_{11}(k)$.

Thus, the Hopf bifurcation curve \mathbf{H}_0 intersects with the Turing bifurcation curve \mathbf{L}_k at

$$(d_{11}^*, \delta^*) = \left(\frac{d_{12} d_{21} \frac{k_*^4}{\ell^4} + (d_{21} - d_{12} \frac{\gamma(4h+1)}{3}) \frac{k_*^2}{\ell^2} - \frac{\gamma(4h+1)}{3}}{d_{22} \frac{k_*^4}{\ell^4}}, \frac{1 - 2h}{\sqrt{3(1+h)}} \right),$$

which is called as the Turing–Hopf bifurcation point.

Next, we continue to verify the transversality condition. Taking d_{11} as a bifurcation parameter and letting $\lambda(d_{11})$ be the root of Eq. (16) near $d_{11} = d_{11}^*$ satisfying $\lambda(d_{11}^*) = 0$. Differentiating the two sides of the characteristic equation (16) with respect to d_{11} , we obtain

$$2\lambda \frac{d\lambda(d_{11})}{dd_{11}} - \left(\frac{dT_k(d_{11})}{dd_{11}} \lambda + T_k \frac{d\lambda(d_{11})}{dd_{11}} \right) + \frac{dD_k(d_{11})}{dd_{11}} = 0.$$

By combining with Eq. (17), we can obtain

$$\frac{d\lambda(d_{11})}{dd_{11}} = \frac{-d_{22} \frac{k_*^4}{\ell^4} - \frac{k_*^2}{\ell^2} \lambda}{2\lambda - T_k}. \tag{24}$$

Moreover, when $\delta > \delta^*$, from the discussion in Sect. 3.1, we know that $a_{11} < 0$. Thus, when $\delta > \delta^*$, we can obtain that

$$T_{k_*} = a_{11} - (d_{11} + d_{22}) \frac{k_*^2}{\ell^2} < 0. \tag{25}$$

By combining with Eqs. (24) and (25), we have

$$\begin{aligned} \operatorname{Re} \left(\frac{d\lambda(d_{11})}{dd_{11}} \Big|_{\mathbf{L}_{k_*}} \right) &= \operatorname{Re} \left(\frac{-d_{22} \frac{k_*^4}{\ell^4} - \frac{k_*^2}{\ell^2} \lambda}{2\lambda - T_k} \Big|_{\mathbf{L}_{k_*}} \right) \\ &= \operatorname{Re} \left(\frac{-d_{22} \frac{k_*^4}{\ell^4}}{-T_{k_*}} \right) = \frac{d_{22} \frac{k_*^4}{\ell^4}}{T_{k_*}} < 0, \end{aligned}$$

where the symbol $\operatorname{Re}(\vartheta)$ represents the real part of ϑ . This, together with the fact that

$$\operatorname{sign} \left(\frac{d\operatorname{Re}(\lambda(d_{11}))}{dd_{11}} \Big|_{\mathbf{L}_{k_*}} \right) = \operatorname{sign} \left(\operatorname{Re} \left(\frac{d\lambda(d_{11})}{dd_{11}} \Big|_{\mathbf{L}_{k_*}} \right) \right) < 0,$$

we have

$$\frac{d\operatorname{Re}(\lambda(d_{11}))}{dd_{11}} \Big|_{\mathbf{L}_{k_*}} < 0,$$

where the symbol sign represents the sign function.

Moreover, if taking δ as a bifurcation parameter, letting $\lambda(\delta) = \alpha(\delta) \pm i\beta(\delta)$ be the pair of roots of Eq. (16) near $\delta = \delta^*$ satisfying $\alpha(\delta^*) = 0$ and $\beta(\delta^*) = \omega_c$, we

have the following transversality condition. Differentiating the two sides of Eq. (16) with respect to δ , we obtain

$$2\lambda \frac{d\lambda(\delta)}{d\delta} - \left(\frac{dT_k(\delta)}{d\delta} \lambda + T_k \frac{d\lambda(\delta)}{d\delta} \right) + \frac{dD_k(\delta)}{d\delta} = 0. \tag{26}$$

By combining with Eqs. (17) and (26), we have

$$\frac{d\lambda(\delta)}{d\delta} = \frac{\left(\lambda + d_{22} \frac{k^2}{\ell^2} \right) \frac{da_{11}}{d\delta} - \left(d_{12} \frac{k^2}{\ell^2} + 1 \right) \frac{da_{21}}{d\delta}}{2\lambda - T_k}. \tag{27}$$

Furthermore, by Eqs. (17) and (27) as well as $T_0(\delta^*) = a_{11}(\delta^*) = 0$ and

$$\left. \frac{da_{11}(\delta)}{d\delta} \right|_{\delta=\delta^*} = \frac{3\gamma(h+1)(2h-1)}{(4h+1)\sqrt{3(h+1)}} > 0,$$

we have

$$\begin{aligned} \operatorname{Re} \left(\left. \frac{d\lambda(\delta)}{d\delta} \right|_{\mathbf{H}_0} \right) &= \operatorname{Re} \left(\frac{i\omega_c \left. \frac{da_{11}}{d\delta} \right|_{\delta=\delta^*} - \left. \frac{da_{21}}{d\delta} \right|_{\delta=\delta^*}}{2i\omega_c - T_0(\delta^*)} \right) \\ &= \frac{1}{2} \left. \frac{da_{11}}{d\delta} \right|_{\delta=\delta^*} = \frac{3\gamma(h+1)(2h-1)}{2(4h+1)\sqrt{3(h+1)}} > 0. \end{aligned}$$

This, together with the fact that

$$\operatorname{sign} \left(\left. \frac{d\operatorname{Re}(\lambda(\delta))}{d\delta} \right|_{\mathbf{H}_0} \right) = \operatorname{sign} \left(\operatorname{Re} \left(\left. \frac{d\lambda(\delta)}{d\delta} \right|_{\delta=\delta^*} \right) \right) > 0,$$

we have

$$\left. \frac{d\operatorname{Re}(\lambda(\delta))}{d\delta} \right|_{\mathbf{H}_0} > 0.$$

Thus, the proof of conclusion (II) is completed. \square

3.3 Bifurcation diagram for system (4) in $d_{11} - \delta$ plane

Taking $\ell = 1, \gamma = 3, h = 0.1, d_{12} = 1, d_{21} = 10, d_{22} = 15$, and by combining with Eqs. (13), (18),

(20), (21), (22) and (23), we can conclude that $k^* = 0, k_* = 1$ and

$$\begin{aligned} \mathbf{H}_0 : \delta &= \frac{1-2h}{\sqrt{3(1+h)}} = 0.4404, \\ a_{21} &= \frac{3(\delta\sqrt{\delta^2+0.4}(2-2\delta^2-0.4) + \delta^2(2-2\delta^2-0.8) + 0.8)}{4(\delta\sqrt{\delta^2+0.4} + \delta^2 + 0.2)}, \\ \mathbf{L} : &\frac{45(\delta^2(-3\delta^2+0.2) + \delta\sqrt{\delta^2+0.4}(-3\delta^2+0.8))}{2\delta\sqrt{\delta^2+0.4} + 2\delta^2 + 0.4} \\ &- 2\sqrt{(15d_{11}-10)a_{21} + 10} - a_{21} = 0, \\ \mathbf{L}_1 : &15d_{11} - \frac{45(\delta^2(-3\delta^2+0.2) + \delta\sqrt{\delta^2+0.4}(-3\delta^2+0.8))}{2\delta\sqrt{\delta^2+0.4} + 2\delta^2 + 0.4} \\ &- 20 + 2a_{21} = 0. \end{aligned}$$

Numerical calculation confirms that when $k_* = 1$, the Turing bifurcation curves \mathbf{L}_1 are tangent to the curve \mathbf{L} at $P_1(-0.0131, 0.8717)$ and $P_2(0.5583, 0.7399)$, see Fig. 2a for details. Moreover, the Hopf bifurcation curve \mathbf{H}_0 intersects with Turing bifurcation curve \mathbf{L}_1 at the point $(d_{11}^*, \delta^*) = (1.1467, 0.4404)$ and system (4) undergoes Turing–Hopf bifurcation near the positive constant equilibrium point $E_*(0.2667, 0.5867)$, see Fig. 2b for details.

4 Normal form for Turing–Hopf bifurcation in the reaction–diffusion system (4)

Notice that the method of computing normal form of general reaction–diffusion system which presented in [34] can be used to obtain the third-order truncated normal form of system (4) by a slight modification. Denote the Turing–Hopf bifurcation point as (d_{11}^*, δ^*) . Introduce the perturbation parameters μ_1 and μ_2 by setting $d_{11} = d_{11}^* + \mu_1$ and $\delta = \delta^* + \mu_2$ such that $(\mu_1, \mu_2) = (0, 0)$ is the Turing–Hopf bifurcation point in the perturbation plane of μ_1 and μ_2 . Then the system (4) becomes

$$\begin{cases} \frac{\partial u}{\partial t} = (d_{11}^* + \mu_1)\Delta u + d_{12}\Delta v + \gamma u(1-u) \\ \quad - \frac{uv}{(\delta^* + \mu_2)\sqrt{u+h}}, & x \in \Omega, t > 0, \\ \frac{\partial v}{\partial t} = d_{21}\Delta u + d_{22}\Delta v - v + \frac{uv}{(\delta^* + \mu_2)\sqrt{u+h}}, \\ \quad x \in \Omega, t > 0. \end{cases} \tag{28}$$

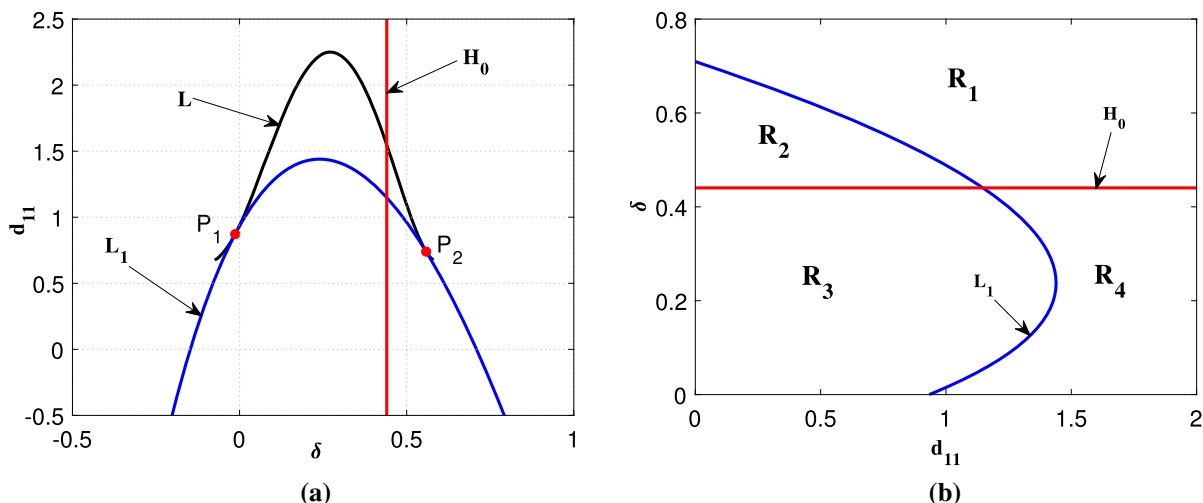


Fig. 2 Bifurcation diagram for system (4) in $d_{11} - \delta$ plane with $k_* = 1$. H_0 denotes the Hopf bifurcation curve, L_1 denotes the Turing bifurcation curve and L is the curve defined by (18). The region R_1 is the stability region of the positive constant equilibrium point E_*

The positive constant equilibrium point of system (28) becomes

$$u_* = \frac{\delta^* + \mu_2}{2} \left(\delta^* + \mu_2 + \sqrt{(\delta^* + \mu_2)^2 + 4h} \right),$$

$$v_* = \lambda u_*(1 - u_*)$$

with $0 < \delta^* + \mu_2 < 1/\sqrt{h+1}$. Making the change of variables by the translation $\bar{u} = u - u_*$ and $\bar{v} = v - v_*$, and dropping the bars, then the system (28) is transformed into

$$\begin{cases} \frac{\partial u}{\partial t} = (d_{11}^* + \mu_1)\Delta u + d_{12}\Delta v + \gamma(u + u_*)(1 - (u + u_*)) \\ \quad - \frac{(u + u_*)(v + v_*)}{(\delta^* + \mu_2)\sqrt{(u + u_*) + h}}, \quad x \in \Omega, \quad t > 0, \\ \frac{\partial v}{\partial t} = d_{21}\Delta u + d_{22}\Delta v - (v + v_*) \\ \quad + \frac{(u + u_*)(v + v_*)}{(\delta^* + \mu_2)\sqrt{(u + u_*) + h}}, \quad x \in \Omega, \quad t > 0. \end{cases} \tag{29}$$

For the system (29), when $\mu_1 = \mu_2 = 0$, $\Delta_0(\lambda) = 0$ has a pair of purely imaginary roots $\pm i\omega_c$, $\Delta_{k_*}(\lambda) = 0$ has a simple zero root $\lambda = 0$ and a negative real root $\lambda = -T_{k_*}$, and if $k \neq 0, k_*$, all roots of $\Delta_k(\lambda) = 0$ have negative real parts.

By the real-valued Hilbert space \mathcal{X} which is defined in Sect. 3, the system (29) can be written as the following abstract ordinary differential equation (ODE), that

librium point E_* , R_2 represents the region of Turing instability, and R_3 and R_4 are the instability region of the positive constant equilibrium point E_*

is

$$\frac{dU(t)}{dt} = d\Delta U + L_0(U) + \tilde{F}(U, \mu) \tag{30}$$

where $U = (u, v)^T$, $\mu = (\mu_1, \mu_2)$, $\tilde{F}(U, \mu) = L(\mu)(U) - L_0(U) + \tilde{d}\Delta u + F(U, \mu)$,

$$d = \begin{pmatrix} d_{11}^* & d_{12} \\ d_{21} & d_{22} \end{pmatrix}, \quad \tilde{d} = \begin{pmatrix} \mu_1 & 0 \\ 0 & 0 \end{pmatrix}, \tag{31}$$

$$L(\mu) = \begin{pmatrix} a_{11}(\delta^* + \mu_2) & -1 \\ a_{21}(\delta^* + \mu_2) & 0 \end{pmatrix}.$$

Here, $a_{11}(\delta^* + \mu_2), a_{21}(\delta^* + \mu_2)$ indicating a_{11} and a_{21} are dependent on $\delta^* + \mu_2$, respectively. Moreover, we have

$$F(U, \mu) = \begin{pmatrix} F^{(1)}(u, v, \mu_1, \mu_2) \\ F^{(2)}(u, v, \mu_1, \mu_2) \end{pmatrix}$$

with

$$F^{(1)}(u, v, \mu_1, \mu_2) = \gamma(u + u_*)(1 - (u + u_*)) - \frac{(u + u_*)(v + v_*)}{(\delta^* + \mu_2)\sqrt{(u + u_*) + h}} - a_{11}(\delta^* + \mu_2)u + v, \tag{32}$$

$$F^{(2)}(u, v, \mu_1, \mu_2) = -(v + v_*) + \frac{(u + u_*)(v + v_*)}{(\delta^* + \mu_2)\sqrt{(u + u_*) + h}} - a_{21}(\delta^* + \mu_2)u.$$

For the formal Taylor expansions of L

$$L(\mu) = L_0 + \mu_1 L_1^{(1,0)} + \mu_2 L_1^{(0,1)} + \frac{1}{2} \left(\mu_1^2 L_2^{(2,0)} + 2\mu_1 \mu_2 L_2^{(1,1)} + \mu_2^2 L_2^{(0,2)} \right) + \dots,$$

and by Eq. (31), we can obtain

$$L_0 = \begin{pmatrix} a_{11}(\delta^*) & -1 \\ a_{21}(\delta^*) & 0 \end{pmatrix}, \quad L_1^{(1,0)} = \begin{pmatrix} 0 & 0 \\ 0 & 0 \end{pmatrix},$$

$$L_1^{(0,1)} = \begin{pmatrix} A & 0 \\ B & 0 \end{pmatrix},$$

where

$$A := \frac{\gamma(-3(u_*)^2 - 6u_*h + h - 2h^2) \left(2\delta + \sqrt{\delta^2 + 4h} + \frac{\delta^2}{\sqrt{\delta^2 + 4h}} \right)}{4(u_* + h)^2},$$

$$B := \frac{\gamma(-h - (u_*)^2 - 2u_*h - 2h^2) \left(2\delta + \sqrt{\delta^2 + 4h} + \frac{\delta^2}{\sqrt{\delta^2 + 4h}} \right)}{4(u_* + h)^2}.$$

Let

$$\mathcal{M}_k(\lambda) = \lambda I_2 - \begin{pmatrix} -d_{11}^* \frac{k^2}{\ell^2} & -d_{12} \frac{k^2}{\ell^2} \\ -d_{21} \frac{k^2}{\ell^2} & -d_{22} \frac{k^2}{\ell^2} \end{pmatrix} - L_0$$

$$= \begin{pmatrix} \lambda + d_{11}^* \frac{k^2}{\ell^2} & d_{12} \frac{k^2}{\ell^2} + 1 \\ d_{21} \frac{k^2}{\ell^2} - \frac{\gamma(4h+1)}{3} & \lambda + d_{22} \frac{k^2}{\ell^2} \end{pmatrix},$$

where I_2 is a 2×2 identity matrix, then by a straightforward calculation, we can obtain that $\xi_0 \in \mathbb{C}^2$ and $\xi_{k_*} \in \mathbb{R}^2$ are the eigenvectors associated with the eigenvalues $i\omega_c$ and 0, respectively, and $\eta_0 \in \mathbb{C}^2$ and $\eta_{k_*} \in \mathbb{R}^2$ are the corresponding adjoint eigenvectors, where

$$\xi_0 = \begin{pmatrix} 1 \\ -i\omega_c \end{pmatrix}, \quad \eta_0 = \frac{1}{2} \begin{pmatrix} 1 \\ i\omega_c \end{pmatrix}, \quad \xi_{k_*} = \begin{pmatrix} 1 \\ -\frac{d_{11}^* \frac{k_*^2}{\ell^2}}{d_{12} \frac{k_*^2}{\ell^2} + 1} \end{pmatrix},$$

$$\eta_{k_*} = \begin{pmatrix} \frac{3d_{21} \frac{k_*^2}{\ell^2} (d_{12} \frac{k_*^2}{\ell^2} + 1) - \gamma(4h+1) (d_{12} \frac{k_*^2}{\ell^2} + 1)}{3d_{21} \frac{k_*^2}{\ell^2} (d_{12} \frac{k_*^2}{\ell^2} + 1) - \gamma(4h+1) (d_{12} \frac{k_*^2}{\ell^2} + 1) + 3(d_{11}^*)^2 \frac{k_*^4}{\ell^4}} \\ -3d_{11}^* \frac{k_*^2}{\ell^2} (d_{12} \frac{k_*^2}{\ell^2} + 1) \\ \frac{3d_{21} \frac{k_*^2}{\ell^2} (d_{12} \frac{k_*^2}{\ell^2} + 1) - \gamma(4h+1) (d_{12} \frac{k_*^2}{\ell^2} + 1) + 3(d_{11}^*)^2 \frac{k_*^4}{\ell^4}} \end{pmatrix},$$

such that

$$\langle \Psi_1, \Phi_1 \rangle = I_2, \quad \langle \Psi_2, \Phi_2 \rangle = 1,$$

where

$$\Phi_1 = (\xi_0, \bar{\xi}_0), \quad \Phi_2 = \xi_{k_*}, \quad \Psi_1 = \text{col} \left(\eta_0^T, \bar{\eta}_0^T \right), \quad \Psi_2 = \eta_{k_*}^T.$$

Here, $\text{col}(\cdot)$ represents the column vector. Furthermore, for vectors $\widehat{\varphi}, \widehat{\psi} \in \mathbb{R}^2$, we define their scalar product as $\langle \widehat{\psi}^T, \widehat{\varphi} \rangle = \widehat{\psi}^T \widehat{\varphi}$.

Notice that the phase space \mathcal{X} can be decomposed as

$$\mathcal{X} = \mathcal{P} \oplus \mathcal{Q}, \quad \mathcal{P} = \text{Im } \pi, \quad \mathcal{Q} = \text{Ker } \pi, \tag{33}$$

where $\dim \mathcal{P} = 3$ and $\pi : \mathcal{X} \mapsto \mathcal{P}$ is the projection defined by

$$\pi(U) = \left(\Phi_1 \left\langle \Psi_1, \left([U, \beta_0^{(1)}], [U, \beta_0^{(2)}] \right)^T \right\rangle \right)^T \beta_0$$

$$+ \left(\Phi_2 \left\langle \Psi_2, \left([U, \beta_{k_*}^{(1)}], [U, \beta_{k_*}^{(2)}] \right)^T \right\rangle \right)^T \beta_{k_*}.$$

According to (33), $U \in \mathcal{X}$ can be decomposed as

$$U = \left(\Phi_1 \begin{pmatrix} z_1 \\ z_2 \end{pmatrix} \right)^T \begin{pmatrix} \beta_0^{(1)} \\ \beta_0^{(2)} \end{pmatrix} + (z_3 \Phi_2)^T \begin{pmatrix} \beta_{k_*}^{(1)} \\ \beta_{k_*}^{(2)} \end{pmatrix} + w$$

$$= (z_1 \xi_0 + z_2 \bar{\xi}_0) \gamma_0(x) + z_3 \xi_{k_*} \gamma_{k_*}(x) + w \tag{34}$$

$$= (\Phi_1, \Phi_2) \begin{pmatrix} z_1 \gamma_0(x) \\ z_2 \gamma_0(x) \\ z_3 \gamma_{k_*}(x) \end{pmatrix} + \begin{pmatrix} w_1 \\ w_2 \end{pmatrix},$$

where $w = \text{col}(w_1, w_2)$ and

$$\begin{pmatrix} z_1 \\ z_2 \end{pmatrix} = \left\langle \Psi_1, \left([U, \beta_0^{(1)}], [U, \beta_0^{(2)}] \right)^T \right\rangle,$$

$$z_3 = \left\langle \Psi_2, \left([U, \beta_{k_*}^{(1)}], [U, \beta_{k_*}^{(2)}] \right)^T \right\rangle.$$

By letting

$$\Phi = (\Phi_1, \Phi_2), \quad z_x = (z_1 \gamma_0(x), z_2 \gamma_0(x), z_3 \gamma_{k_*}(x))^T,$$

Equation (34) can be rewritten as

$$U = \Phi z_x + w.$$

For the simplicity of notation, we denote

$$\begin{pmatrix} [\tilde{F}, \beta_v^{(1)}] \\ [\tilde{F}, \beta_v^{(2)}] \end{pmatrix}_{v=0}^{v=k_*} = \text{col} \left(\begin{pmatrix} [\tilde{F}, \beta_0^{(1)}] \\ [\tilde{F}, \beta_0^{(2)}] \end{pmatrix}, \begin{pmatrix} [\tilde{F}, \beta_{k_*}^{(1)}] \\ [\tilde{F}, \beta_{k_*}^{(2)}] \end{pmatrix} \right),$$

and if let $\mathcal{L}U := d\Delta U + L_0(U)$ and denote by \mathcal{L}_1 the restriction of \mathcal{L} to \mathcal{Q} , then system (30) is equivalent to a system of abstract ordinary differential equations (ODEs) in $\mathbb{R}^3 \times \mathcal{Q}$, with finite- and infinite-dimensional variables also separated in the linear term. That is,

$$\begin{cases} \dot{z} = Bz + \Psi \begin{pmatrix} [\tilde{F}(z, w, \mu), \beta_v^{(1)}] \\ [\tilde{F}(z, w, \mu), \beta_v^{(2)}] \end{pmatrix}_{v=0}^{v=k_*}, \\ \dot{w} = \mathcal{L}_1(w) + H(z, w, \mu), \end{cases}$$

where

$$z = (z_1, z_2, z_3)^T, B = \text{diag} \{i\omega_c, -i\omega_c, 0\},$$

$$\Psi = \text{diag} \{\Psi_1, \Psi_2\}, \tilde{F}(z, w, \mu) = \tilde{F}(\Phi z_x + w, \mu),$$

and

$$H(z, w, \mu) = \tilde{F}(z, w, \mu) - \left(\left\langle \eta_0^T, \begin{pmatrix} \tilde{F}(z, w, \mu, \beta_0^{(1)}) \\ \tilde{F}(z, w, \mu, \beta_0^{(2)}) \end{pmatrix} \right\rangle \xi_0 \right. \\ \left. + \left\langle \bar{\eta}_0^T, \begin{pmatrix} \tilde{F}(z, w, \mu, \beta_0^{(1)}) \\ \tilde{F}(z, w, \mu, \beta_0^{(2)}) \end{pmatrix} \right\rangle \bar{\xi}_0 \right) \gamma_0(x) \\ - \left\langle \eta_{k_*}^T, \begin{pmatrix} \tilde{F}(z, w, \mu, \beta_{k_*}^{(1)}) \\ \tilde{F}(z, w, \mu, \beta_{k_*}^{(2)}) \end{pmatrix} \right\rangle \xi_{k_*} \gamma_{k_*}(x).$$

According to [34], by a recursive transformation, the authors obtain that the normal form for Turing–Hopf bifurcation in system (30) reads as

$$\dot{z} = Bz \\ + \begin{pmatrix} B_{11}\mu_1 z_1 + B_{21}\mu_2 z_1 \\ \bar{B}_{11}\mu_1 z_1 + \bar{B}_{21}\mu_2 z_1 \\ B_{13}\mu_1 z_3 + B_{23}\mu_2 z_3 \end{pmatrix} \\ + \begin{pmatrix} B_{210}z_1^2 z_2 + B_{102}z_1 z_3^2 \\ \bar{B}_{210}z_1 z_2^2 + \bar{B}_{102}z_2 z_3^2 \\ B_{111}z_1 z_2 z_3 + B_{003}z_3^3 \end{pmatrix} \\ + O(|z||\mu|^2 + |z|^2|\mu| + |z|^4).$$

The normal form (35) can be written in real coordinates \tilde{v} through the change of variables $z_1 = \tilde{v}_1 - i\tilde{v}_2, z_2 = \tilde{v}_1 + i\tilde{v}_2, z_3 = \tilde{v}_3$, and then changing to cylindrical coordinates by $\tilde{v}_1 = \rho \cos \Theta, \tilde{v}_2 = \rho \sin \Theta, \tilde{v}_3 = \varsigma$, we obtain, truncating at third-order terms and removing the azimuthal term

$$\dot{\rho} = \alpha_1(\mu)\rho + \kappa_{11}\rho^3 + \kappa_{12}\rho\varsigma^2, \\ \dot{\varsigma} = \alpha_2(\mu)\varsigma + \kappa_{21}\rho^2\varsigma + \kappa_{22}\varsigma^3,$$

where

$$\alpha_1(\mu) = \text{Re}(B_{11})\mu_1 + \text{Re}(B_{21})\mu_2, \\ \alpha_2(\mu) = B_{13}\mu_1 + B_{23}\mu_2, \\ \kappa_{11} = \text{Re}(B_{210}), \kappa_{12} = \text{Re}(B_{102}), \kappa_{21} = B_{111}, \\ \kappa_{22} = B_{003}.$$

According to Section 8.6 in [38], we know that the third-order truncated normal form (36) is exactly the same to the third-order truncated normal form of the four-dimensional smooth system depending on two

parameters with Hopf–Hopf bifurcation. For the so-called simple case [38], i.e. $\kappa_{11}\kappa_{22} > 0$, the dynamics of system (4) near the bifurcation value is topologically equivalent to that of normal form (36). However, for the “difficult” cases, the original system (4) is never topologically equivalent to the truncated normal form (36). In general, for the “difficult” cases, in order to obtain the whole dynamics of the original (4), five-order or higher-order normal form needs to be calculated.

With the help of MATLAB software, the explicit values of the coefficients $B_{11}, B_{21}, B_{13}, B_{23}, B_{210}, B_{102}, B_{111}$ and B_{003} can be obtained for the fixed parameters. Notice that the formulas which are used to calculate the above coefficients are rather complicated and we leave them in “Appendix”.

5 Numerical simulations

In this section, the third-order truncated normal form is obtained under the given parameters and some numerical simulations are made to support the results of our theoretical analysis. More precisely, some numerical simulations about the temporal patterns, spatial patterns and spatiotemporal patterns are given.

Let $\Omega = (0, \pi)$ and $\gamma = 3, h = 0.1, d_{12} = 1, d_{21} = 10, d_{22} = 15$, then the system (4) at least undergoes Turing–Hopf bifurcation at the point (1.1467, 0.4404). By using the above-given parameters, the normal form truncated to the third-order terms is

$$\dot{\rho} = -1.5571\mu_2\rho - 1.0401\rho^3 - 1.4138\rho\varsigma^2, \\ \dot{\varsigma} = (0.9290\mu_1 - 2.5716\mu_2)\varsigma \\ - 3.3790\rho^2\varsigma - 2.4380\varsigma^3,$$

where μ_1 and μ_2 are perturbation parameters for the Turing–Hopf bifurcation point (1.1467, 0.4404). Notice that $\rho > 0$ and ς is arbitrary real number. System (37) has a zero equilibrium point $A_0(0, 0)$ for any $\mu_1, \mu_2 \in \mathbb{R}$, three boundary equilibrium points

$$A_1 \left(\sqrt{\frac{-1.5571\mu_2}{1.0401}}, 0 \right), \text{ for } -1.5571\mu_2 > 0, \\ A_2^\pm \left(0, \pm \sqrt{\frac{0.9290\mu_1 - 2.5716\mu_2}{2.4380}} \right),$$

for $0.9290\mu_1 - 2.5716\mu_2 > 0$, and two interior equilibrium points

Table 1 The twelve unfoldings of (36)

Cases	Ia	Ib	II	III	IVa	IVb	V	VIa	VIb	VIIa	VIIb	VIII
d	+1	+1	+1	+1	+1	+1	−1	−1	−1	−1	−1	−1
b	+	+	+	−	−	−	+	+	+	−	−	−
c	+	+	−	+	−	−	+	−	−	+	+	−
$d - bc$	+	−	+	+	+	−	−	+	−	+	−	−

Table 2 The corresponding relationship between the equilibrium points of (37) and the solutions of original system (4)

Equilibrium points of (37)	Solutions of the original system (4)
A_0	Positive constant steady state
A_1	Spatially homogeneous periodic solution
A_2^\pm	Two spatially inhomogeneous steady states with $\cos x$ -like shape in space
A_3^\pm	Two spatially inhomogeneous periodic solutions with $\cos x$ -like shape in space

$$A_3^\pm \left(\sqrt{\frac{1.3134\mu_1 + 0.1605\mu_2}{2.2415}}, \pm \sqrt{\frac{-0.9663\mu_1 - 2.5867\mu_2}{2.2415}} \right)$$

for $1.3134\mu_1 + 0.1605\mu_2 > 0$ and $-0.9663\mu_1 - 2.5867\mu_2 > 0$.

Define the critical bifurcation lines are as follows:

- $H_0 : \mu_2 = 0,$
- $L_1 : \mu_2 = 0.3613\mu_1,$
- $T_1 : \mu_2 = -8.1832\mu_1, \mu_1 > 0,$
- $T_2 : \mu_2 = -0.3736\mu_1, \mu_1 > 0.$

These four lines divide the $\mu_1 - \mu_2$ parameter plane into six regions marked as $D_j, j = 1, 2, \dots, 6$.

Based on Section 7.5 in [39], by the different signs of $d, b, c, d - bc$ in Table 1, the system (36) has twelve distinct types of unfoldings, which are twelve essentially distinct types of phase portraits and bifurcation diagrams. More precisely, for the system (37), we have $d = +1, b = 1.3593 > 0, c = 1.3860 > 0, d - bc = -0.8840 < 0$. That is, the unfolding of the planner system (37) corresponding to the Case Ib in Table 1. Thus, the phase portraits and bifurcation diagrams corresponding to Case Ib can be given out, see Fig. 7.5.2 in Section 7.5 in [39] for details.

The dynamics of the original reaction–diffusion system (4) can be determined by the third-order truncated normal form (37) near the neighbourhood of the Turing–Hopf bifurcation point. According to [34], the

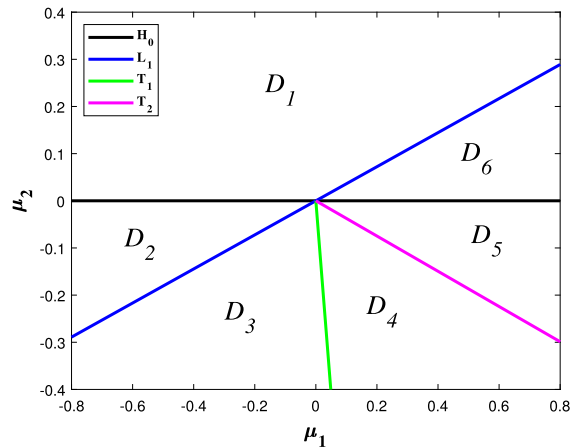


Fig. 3 Bifurcation diagram of the system (4) near the Turing–Hopf bifurcation point (1.1467, 0.4404)

corresponding relationships between the equilibrium points of plane system (37) and the solutions of original system (4) are shown in Table 2.

Furthermore, by the defined critical bifurcation lines, the bifurcation diagram in the $\mu_1 - \mu_2$ parameter plane is shown in Fig. 3. The linearized equation of the system (37) at each equilibrium point is

$$\frac{d}{dt} \begin{pmatrix} \rho \\ \varsigma \end{pmatrix} = \begin{pmatrix} C_1 & -2.8276\rho_i\varsigma_i \\ -6.7580\rho_i\varsigma_i & C_2 \end{pmatrix} \begin{pmatrix} \rho \\ \varsigma \end{pmatrix}, \tag{38}$$

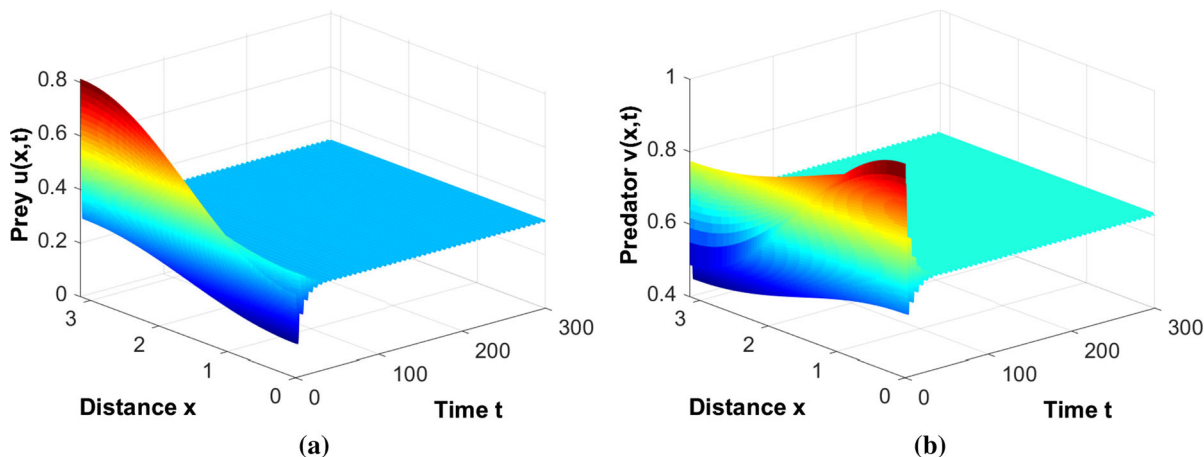


Fig. 4 When $(\mu_1, \mu_2) = (0.60, 0.25)$ lies in region D_1 and let $d_{11} = 1.1467, \delta = 0.5004$, the positive constant steady state $E_*(0.5615, 0.7386)$ is asymptotically stable. The initial value is $u(x, 0) = 0.5615 - 0.25 \cos(x), v(x, 0) = 0.7386 + 0.25 \cos x$

where

$$C_1 := -1.5571\mu_2 - 3.1203\rho_i^2 - 1.4138\zeta_i^2,$$

$$C_2 := 0.9290\mu_1 - 2.5716\mu_2 - 3.3790\rho_i^2 - 7.3140\zeta_i^2$$

with $i = 1, 2, 3, 4$ and

$$(\rho_1, \zeta_1) = A_0, (\rho_2, \zeta_2) = A_1,$$

$$(\rho_3, \pm\zeta_3) = A_2^\pm, (\rho_4, \pm\zeta_4) = A_3^\pm.$$

More precisely, the coefficient matrices of linearized equation (38) at equilibrium points $A_0, A_1, A_2^\pm, A_3^\pm$ are

$$J(A_0) = \begin{pmatrix} -1.5571\mu_2 & 0 \\ 0 & 0.9290\mu_1 - 2.5716\mu_2 \end{pmatrix},$$

$$J(A_1) = \begin{pmatrix} 3.1142\mu_2 & 0 \\ 0 & 0.9290\mu_1 + 2.4870\mu_2 \end{pmatrix},$$

$$J(A_2^\pm) = \begin{pmatrix} -0.5387\mu_1 - 0.0658\mu_2 & 0 \\ 0 & -1.8580\mu_1 + 5.1432\mu_2 \end{pmatrix},$$

$$J(A_3^\pm) = \begin{pmatrix} -1.2188\mu_1 - 0.1490\mu_2 & C_3 \\ C_4 & 2.1021\mu_1 + 5.6268\mu_2 \end{pmatrix},$$

respectively, where

$$C_3 := \mp 2.8276\sqrt{-0.2526\mu_1^2 - 0.0826\mu_2^2 - 0.7070\mu_1\mu_2},$$

$$C_4 := \mp 6.7580\sqrt{-0.2526\mu_1^2 - 0.0826\mu_2^2 - 0.7070\mu_1\mu_2}.$$

By combining with the bifurcation diagram in Fig. 3 and the linear stability theory, we can analyse the sign of the eigenvalues corresponding to the characteristic equations; thus, the stability and instability of each equilibrium point in regions D_1 - D_6 can be obtained.

In region D_1 , the third-order truncated normal form (37) has only one equilibrium point A_0 and it is asymptotically stable. This implies that the positive constant steady state E_* of the original system (4) is asymptotically stable, as shown in Fig. 4 for $(\mu_1, \mu_2) = (0.60, 0.25)$ and the initial value $u(x, 0) = 0.5615 - 0.25 \cos(x), v(x, 0) = 0.7386 + 0.25 \cos x$.

In region D_2 , the third-order truncated normal form (37) has two equilibrium points: A_0 and A_1 . The equilibrium point A_0 is unstable and the equilibrium point A_1 is asymptotically stable. This means that the system (4) has a stable spatially homogeneous periodic solution. For $(\mu_1, \mu_2) = (-0.28, -0.1)$ and initial value $u(x, 0) = 0.1802 + 0.01 \cos(x), v(x, 0) = 0.4431 + 0.01 \cos x$, Fig. 5 illustrates this result.

In region D_3 , the third-order truncated normal form (37) has four equilibrium points: A_0, A_1, A_2^+ and A_2^- . The equilibrium points A_0, A_2^+ and A_2^- are unstable and the equilibrium point A_1 is asymptotically stable. Thus, the original system (4) has an unstable positive constant steady state, two unstable spatially inhomogeneous steady states like $\cos x$ -shape in space, and a stable spatially homogeneous periodic solution. By choosing $(\mu_1, \mu_2) = (-0.16, -0.08)$ and the initial value $u(x, 0) = 0.1961 + 0.2 \cos x, v(x, 0) = 0.4729 + 0.2 \cos x$, the dynamics of the original system (4) evolves from the spatially inhomogeneous steady states to the spatially homogeneous periodic solution, as shown in Fig. 6.

In region D_4 , the third-order truncated normal form (37) has six equilibrium points: A_0, A_1, A_2^\pm and A_3^\pm .

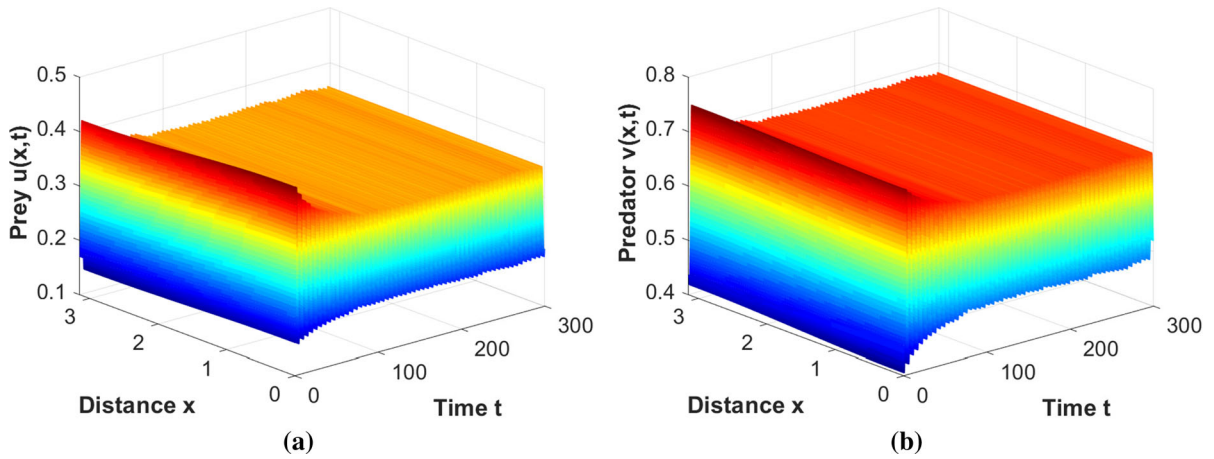


Fig. 5 When $(\mu_1, \mu_2) = (-0.28, -0.1)$ lies in region D_2 and let $d_{11} = 1.1467, \delta = 0.4404$, the positive constant steady state $E_*(0.1802, 0.4431)$ is unstable and there is a stable spatially

homogeneous periodic solution. The initial value is $u(x, 0) = 0.1802 + 0.01 \cos(x), v(x, 0) = 0.4431 + 0.01 \cos x$

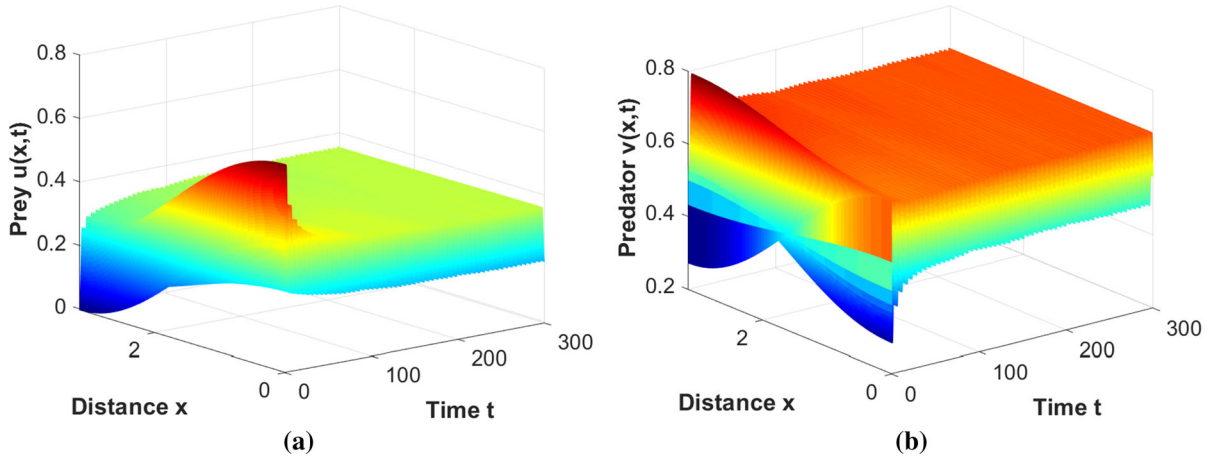


Fig. 6 When $(\mu_1, \mu_2) = (-0.16, -0.08)$ lies in region D_3 and let $d_{11} = 1.1400, \delta = 0.4404$, the positive constant steady state $E_*(0.1961, 0.4729)$ is unstable and there is a heteroclinic orbit

connecting the unstable spatially inhomogeneous steady state to stable spatially homogeneous periodic solution. The initial value is $u(x, 0) = 0.1961 + 0.2 \cos x, v(x, 0) = 0.4729 + 0.2 \cos x$

The equilibrium point A_0 is unstable, the equilibrium points A_1, A_2^\pm and A_3^\pm are asymptotically stable. This implies that the original system (4) has an unstable positive constant steady state, a stable spatially homogeneous periodic solution, two stable spatially inhomogeneous steady states like $\cos x$ -shape in space and two stable spatially inhomogeneous periodic solution like $\cos x$ -shape in space. Taking the parameter $(\mu_1, \mu_2) = (0.005, -0.002)$ and the initial value $u(x, 0) = 0.2648 - 0.1 \cos x, v(x, 0) = 0.5840 - 0.15 \cos x$ close to the unstable positive con-

stant steady state, the dynamics of the original system (4) evolves from unstable spatially inhomogeneous steady states, spatially inhomogeneous periodic solution to stable spatially homogeneous periodic solution, as shown in Fig. 7. Furthermore, by taking the parameter $(\mu_1, \mu_2) = (0.23, -0.09)$ and the initial value $u(x, 0) = 0.1881 - 0.02 \cos x, v(x, 0) = 0.4581 - 0.02 \cos x$ close to the unstable positive constant steady state, the dynamics of the original system (4) evolves from unstable spatially inhomogeneous steady states

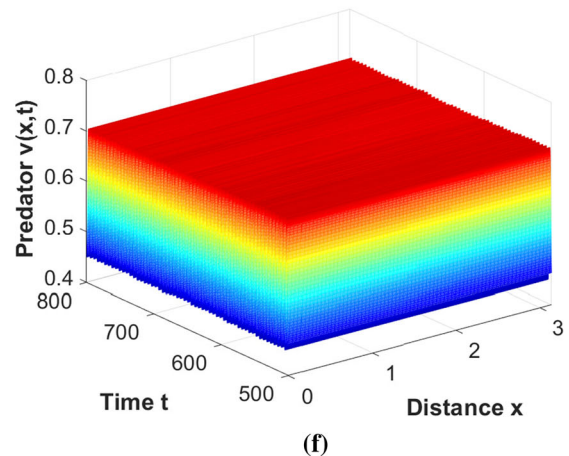
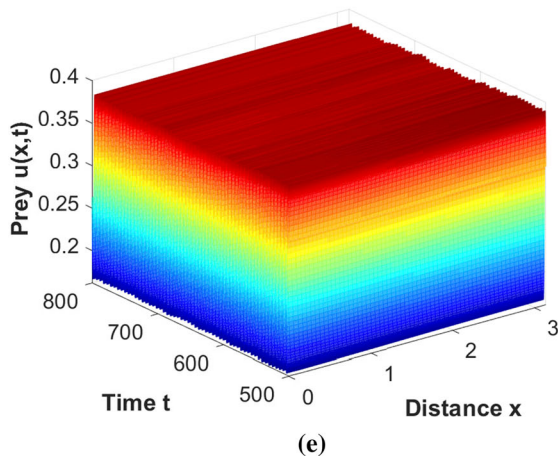
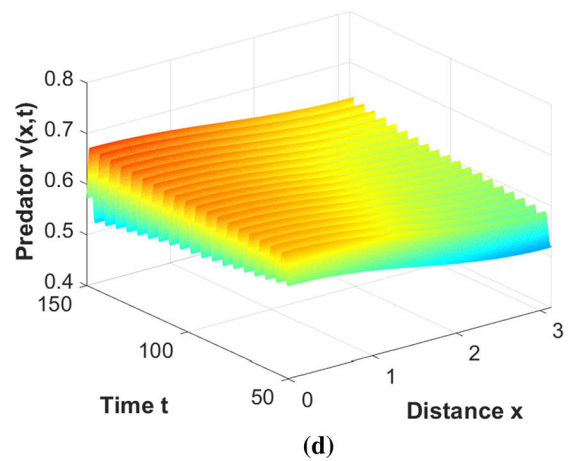
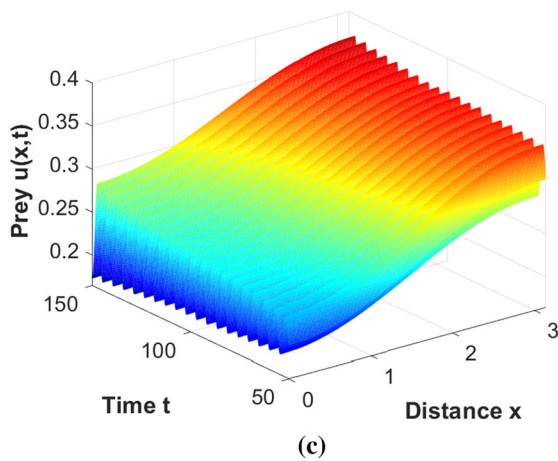
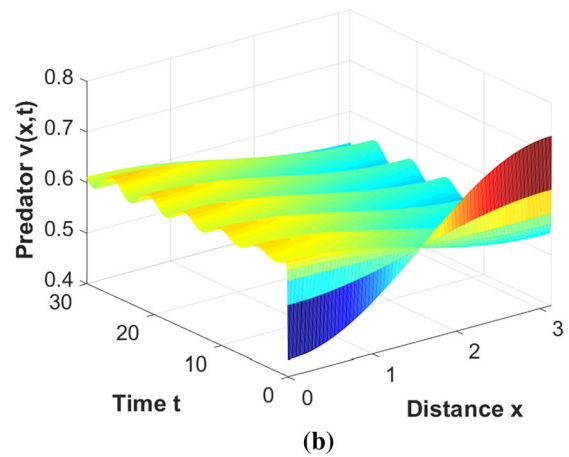
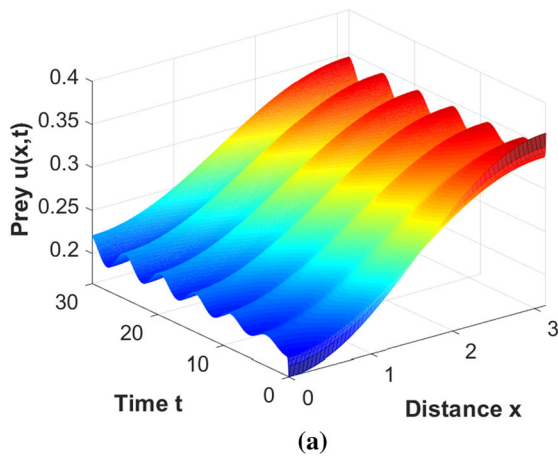


Fig. 7 When $(\mu_1, \mu_2) = (0.005, -0.002)$ lies in region D_4 and let $d_{11} = 1.1467$, $\delta = 0.4364$, the positive constant steady state $E_*(0.2648, 0.5840)$ is unstable and there is a heteroclinic orbit connecting the spatially inhomogeneous periodic solution to stable spatially homogeneous periodic solution. The initial value is

$u(x, 0) = 0.2648 - 0.1 \cos x$, $v(x, 0) = 0.5840 - 0.15 \cos x$. **a** and **b** are transient behaviours for u and v , respectively; **c** and **d** are middle-term behaviours for u and v , respectively; **e** and **f** are long-term behaviours for u and v , respectively

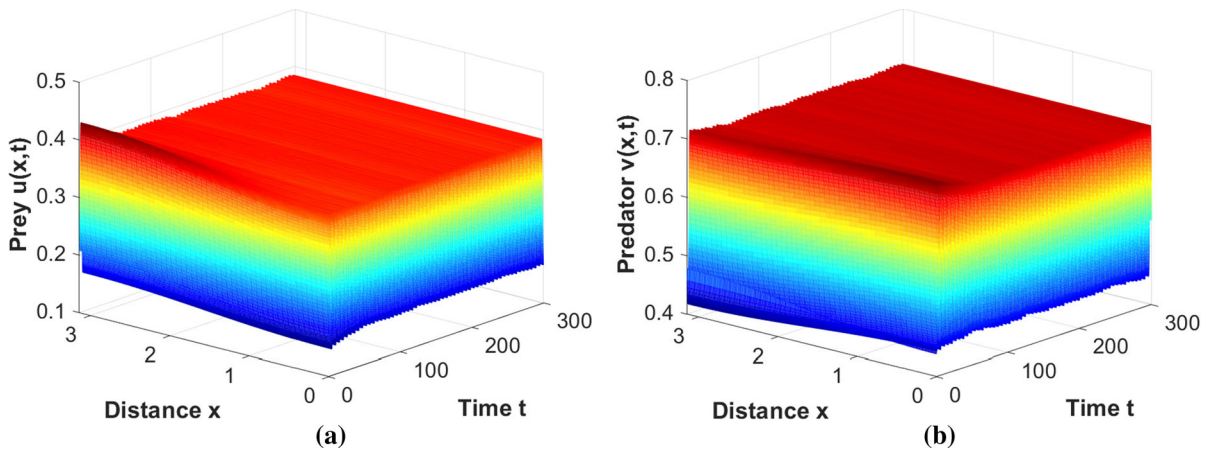


Fig. 8 When $(\mu_1, \mu_2) = (0.23, -0.09)$ lies in region D_4 and let $d_{11} = 1.1467, \delta = 0.4364$, the positive constant steady state $E_*(0.1881, 0.4581)$ is unstable and there is stable spatially

homogeneous periodic solution. The initial value is $u(x, 0) = 0.1881 - 0.02 \cos x, v(x, 0) = 0.4581 - 0.02 \cos x$

to stable spatially homogeneous periodic solution, as shown in Fig. 8.

In region D_5 , the third-order truncated normal form has four equilibrium points: A_0, A_1, A_2^+ and A_2^- . The equilibrium point A_0 is unstable and the equilibrium points A_1, A_2^+ and A_2^- are asymptotically stable. Thus, the original system (4) has an unstable positive constant steady state, a stable spatially homogeneous periodic solution and two stable spatially inhomogeneous steady states like $\cos x$ -shape in space. Taking the parameter $(\mu_1, \mu_2) = (0.17, -0.03)$ and the initial value $u(x, 0) = 0.2389 - 0.15 \cos x, v(x, 0) = 0.5455 - 0.15 \cos x$ close to the unstable positive constant steady state, the dynamics of the original system (4) evolves from unstable positive constant steady state to stable spatially homogeneous periodic solution, as shown in Fig. 9a and b. Taking the parameter $(\mu_1, \mu_2) = (0.31, -0.05)$ and the initial value $u(x, 0) = 0.2213 - 0.2 \cos x, v(x, 0) = 0.5169 + 0.2 \cos x$ close to the unstable positive constant steady state, the dynamics of the original system (4) evolves from unstable positive constant steady state to stable spatially inhomogeneous steady states, as shown in Fig. 9c and d.

In region D_6 , the third-order truncated normal form (37) has three equilibrium points: A_0, A_2^+ and A_2^- . The equilibrium point A_0 is unstable and the equilibrium points A_2^+ and A_2^- are asymptotically stable. Thus, the original system (4) has an unstable positive con-

stant steady state and two stable non-constant steady states like $\cos x$ -shape in space. For the fixed parameter $(\mu_1, \mu_2) = (0.75, 0.1675)$ and choosing different initial values, the original system (4) can converge to one of these two stable non-constant steady states, as shown in Fig. 10a and b for the initial value $u(x, 0) = 0.4514 - 0.15 \cos x, v(x, 0) = 0.7429 + 0.15 \cos x$ and Fig. 10c and d for the initial value $u(x, 0) = 0.4514 + 0.15 \cos x, v(x, 0) = 0.7429 - 0.15 \cos x$.

6 Conclusion and discussion

In this paper, a predator–prey model with cross-diffusion considering the prey individual behaviour and herd behaviour transition with homogeneous Neumann boundary condition is investigated. We first show that the non-negativity and boundedness of solutions corresponding to the model without self-diffusion and cross-diffusion and the model with self-diffusion and cross-diffusion. Then we show the existence and priori boundedness of solutions corresponding to the spatiotemporal model without cross-diffusion. In order to classify the possible dynamical classification near the Turing–Hopf bifurcation point, by using the method of computing the normal form presented in [34], the third-order truncated normal form (37) is given. By the obtained third-order truncated normal form (37), we obtain a zero equilibrium point corresponding to the positive constant steady state of the original sys-

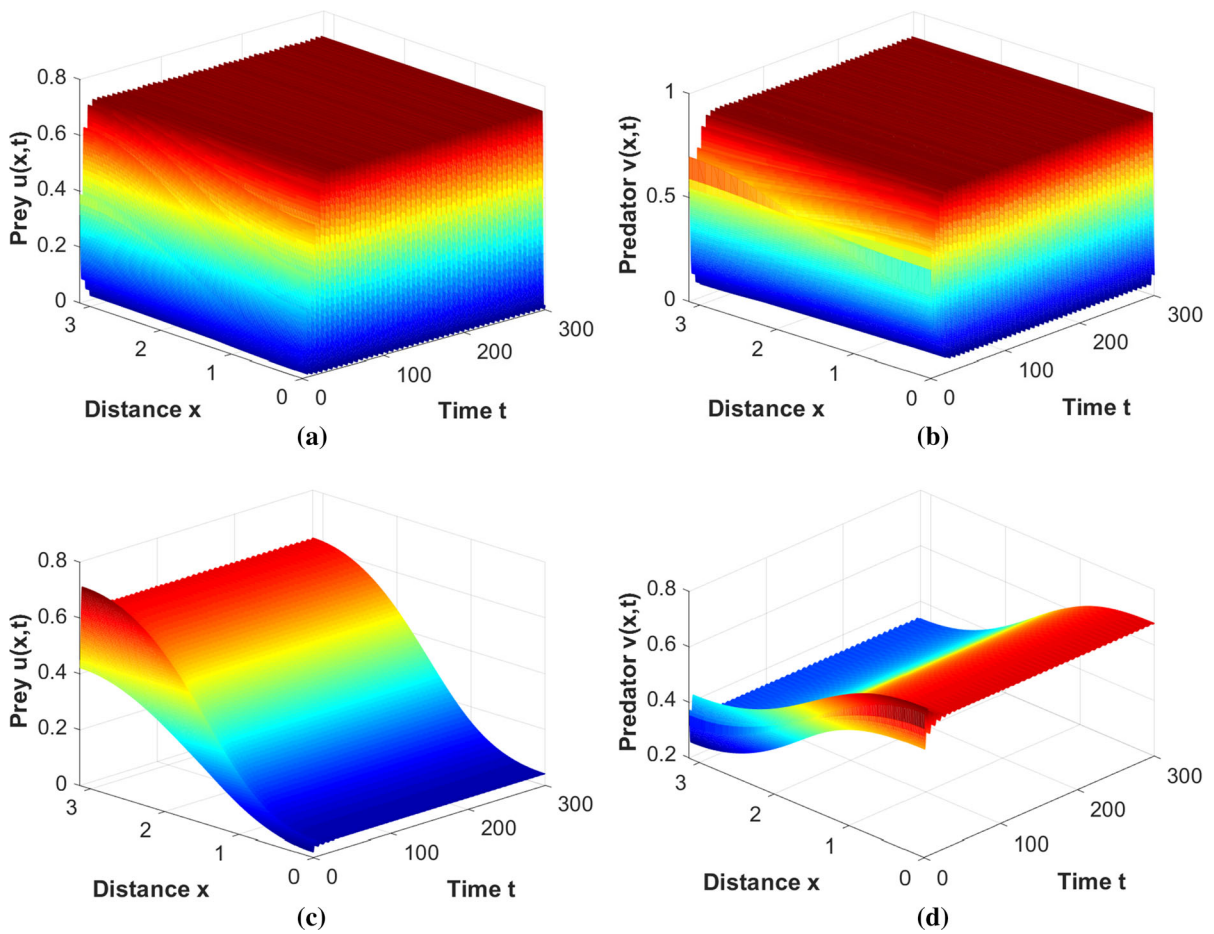


Fig. 9 When $(\mu_1, \mu_2) = (0.17, -0.03)$ lies in region D_5 and let $d_{11} = 1.1467, \delta = 0.3$, the positive constant steady state $E_*(0.2389, 0.5455)$ is unstable and there is a heteroclinic orbit connecting the unstable positive constant steady state to stable spatially homogeneous periodic solution. The initial value is $u(x, 0) = 0.2389 - 0.15 \cos x, v(x, 0) = 0.5455 - 0.15 \cos x$.

When $(\mu_1, \mu_2) = (0.31, -0.05)$ lies in region D_5 and let $d_{11} = 0.9, \delta = 0.4004$, the positive constant steady state $E_*(0.2213, 0.5169)$ is unstable and there is a heteroclinic orbit connecting the unstable positive constant steady state to stable spatially inhomogeneous steady states. The initial value is $u(x, 0) = 0.2213 - 0.2 \cos x, v(x, 0) = 0.5169 + 0.2 \cos x$

tem (4), three boundary equilibrium points A_1 and A_2^\pm in which A_1 corresponding to the spatially homogeneous periodic solution of the original system (4) and A_2^\pm corresponding to the two spatially inhomogeneous steady states with $\cos x$ -like shape in space of the original system (4). Furthermore, two interior equilibrium points A_3^\pm is also obtained corresponding to the two spatially inhomogeneous periodic solutions with $\cos x$ -like shape in space of the original system (4). Moreover, we obtain four inequality which is used to ensure the existence of these different types of equilibrium points. Notice that the four inequality can be seen as the four critical bifurcation lines; thus, by the defined critical

bifurcation lines, the bifurcation diagram in the μ_1 - μ_2 parameters plane which includes six different regions is shown in Fig. 3.

By the numerical simulations, the rich dynamics such as the positive constant steady state, the spatially homogeneous periodic solution, spatially inhomogeneous steady states and spatially inhomogeneous periodic solutions have been found, which can be seen in Figs. 4, 5, 6, 7, 8, 9 and 10. Especially, we would like to mention that the interaction between the Turing bifurcation curve and the Hopf bifurcation curve may leads to the emergence of the spatially inhomogeneous periodic solutions, see Fig. 7a and b for details.

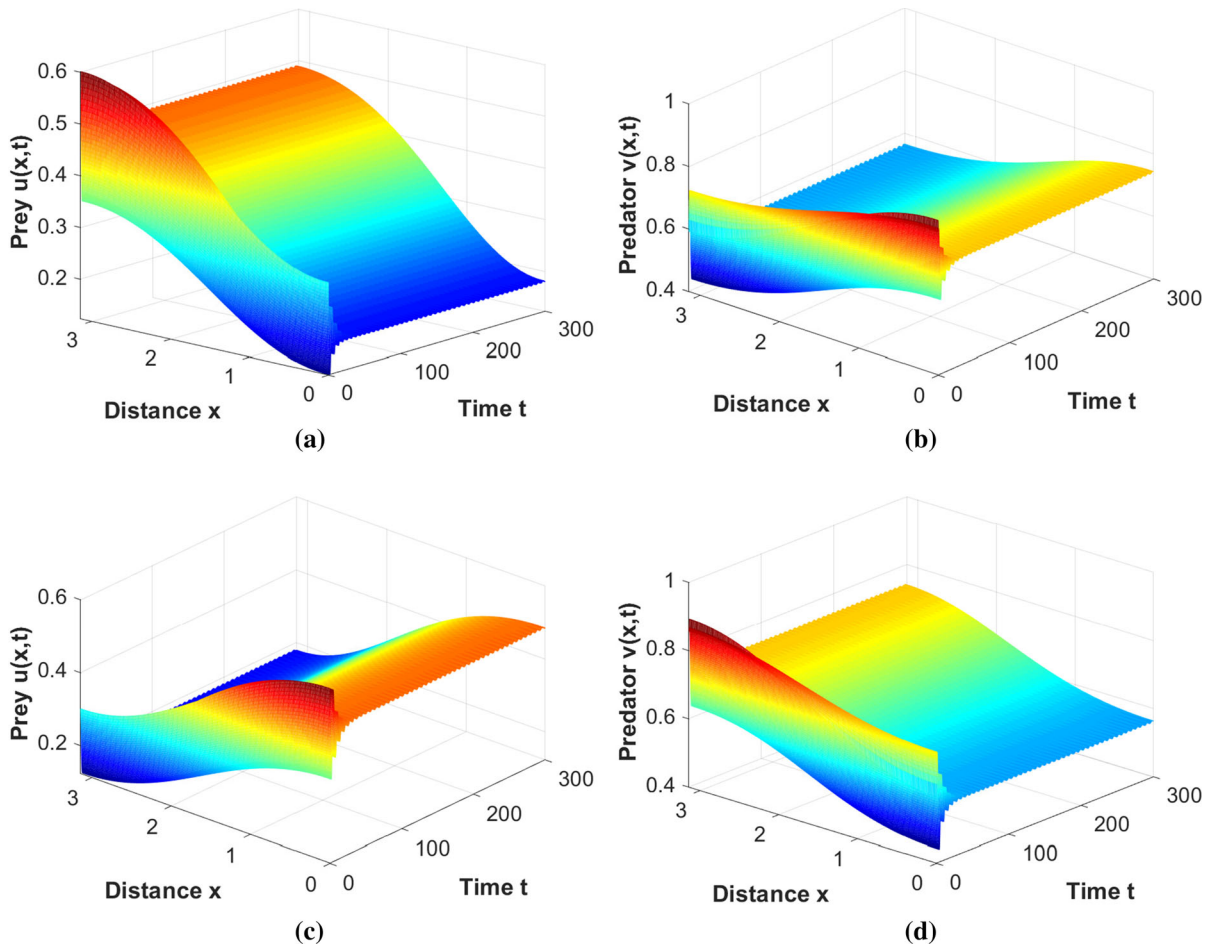


Fig. 10 When $(\mu_1, \mu_2) = (0.75, 0.1675)$ lies in region D_6 and let $d_{11} = 0.9, \delta = 0.5004$, the positive constant steady state $E_+(0.4514, 0.7429)$ is unstable and there are two stable spatially inhomogeneous steady states like $\cos x$ in space. **a** and **b**:

the initial value is $u(x, 0) = 0.4514 - 0.15 \cos x, v(x, 0) = 0.7429 + 0.15 \cos x$; **c** and **d**: the initial value is $u(x, 0) = 0.4514 + 0.15 \cos x, v(x, 0) = 0.7429 - 0.15 \cos x$

We have to point out the fact that the method of computing normal form developing in this paper can also be used to the case without cross-diffusion by a slight modification. Furthermore, in order to the simplicity of notation for further normal form computation and for the convenience of carrying out the numerical simulations, we let $\Omega := (0, \pi)$. However, the spatial Ω can also be taken $(0, \ell\pi)$ with $\ell \in \mathbb{R}^+$. Notice also that the general open interval (\tilde{a}, \tilde{b}) can be transformed to $(0, \pi)$ by a translation and rescaling.

Acknowledgements The authors are grateful to the anonymous referees for their useful suggestions which improve the contents of this article.

Author contributions This research did not involve human participants and animals. This manuscript is investigated and written by YL.

Funding This research did not receive any specific grant from funding agencies in the public, commercial, or not-for-profit sectors.

Code availability The numerical simulations in this paper are carried by using the MATLAB software.

Declarations

Conflict of interest The authors declare that they have no conflict of interest, whether financial or non-financial.

Ethical approval The author agrees to submit this manuscript to Nonlinear Dynamics. Once the submitted manuscript is accepted, the author agrees to publish it in Nonlinear Dynamics.

Appendix

In Sect. 1, we have pointed out that the procedure of computing B_{11} and B_{13} needs to be deduced again. In the following, the detailed derivation process of B_{11} and B_{13} is given. Following Section 3.1.1 in [34], by considering the formal Taylor expansion

$$L(\mu) = L_0 + \mu_1 L_1^{(1,0)} + \mu_2 L_1^{(0,1)} + \frac{1}{2} \left(\mu_1^2 L_2^{(2,0)} + 2\mu_1 \mu_2 L_2^{(1,1)} + \mu_2^2 L_2^{(0,2)} \right) + \dots,$$

$$F(\Phi z_x + w, \mu) = \frac{1}{2} F_2(\Phi z_x + w, \mu) + \frac{1}{3!} F_3(\Phi z_x + w, \mu) + \dots,$$

where $F_j(\Phi z_x + w, \mu)$, $j \geq 2$ is the j -th Fréchet derivative of $F(\Phi z_x + w, \mu)$. For simplicity, we set

$$\mathcal{H} \left(\alpha z_1^{q_1} z_2^{q_2} z_3^{q_3} \mu_1^{l_1} \mu_2^{l_2} \right) = \begin{pmatrix} \alpha z_1^{q_1} z_2^{q_2} z_3^{q_3} \mu_1^{l_1} \mu_2^{l_2} \\ \bar{\alpha} z_1^{q_2} z_2^{q_1} z_3^{q_3} \mu_1^{l_1} \mu_2^{l_2} \end{pmatrix}, \alpha \in \mathbb{C}.$$

Furthermore, we have

$$f_2^1(z, 0, \mu) = \psi \left(\begin{bmatrix} 2\tilde{L}_1(\mu)(\Phi z_x) + F_2(\Phi z_x, \mu), \beta_v^{(1)} \\ 2\tilde{L}_1(\mu)(\Phi z_x) + F_2(\Phi z_x, \mu), \beta_v^{(2)} \end{bmatrix} \right)_{v=0}^{v=k_*},$$

where $\tilde{L}_1(\mu) = \mu_1 L_1^{(1,0)} + \mu_2 L_1^{(0,1)} + \tilde{d}\Delta$, and \tilde{d} is defined by Eq. (31). Since $F(0, \mu) = 0$ and $DF(0, \mu) = 0$, $F_2(\Phi z_x + w, \mu)$ can be written as follows

$$F_2(\Phi z_x + w, \mu) = F_2(\Phi z_x + w, 0) = \sum_{q_1+q_2+q_3=2} A_{q_1 q_2 q_3} \gamma_0^{q_1+q_2} (x) \gamma_{k_*}^{q_3} (x) z_1^{q_1} z_2^{q_2} z_3^{q_3} + \mathcal{S}_2(\Phi z_x, w) + O(|w|^2),$$

where $q_1, q_2, q_3 \in \mathbb{N}_0$, $\mathcal{S}_2(\Phi z_x, w)$ is the product term of Φz_x and w , and

$$A_{q_1 q_2 q_3} = \left(A_{q_1 q_2 q_3}^{(1)}, A_{q_1 q_2 q_3}^{(2)} \right)^T \in \mathbb{R}^2.$$

Here, $A_{q_1 q_2 q_3} = \bar{A}_{q_2 q_1 q_3}$, and $\bar{A}_{q_2 q_1 q_3}$ represents the conjugation of $A_{q_2 q_1 q_3}$.

Noticing the fact that

$$\int_0^{\ell\pi} \gamma_0^2(x) \gamma_{k_*}(x) dx = \int_0^{\ell\pi} \gamma_{k_*}^3(x) dx = 0,$$

$$\int_0^{\ell\pi} \gamma_0^2(x) dx = 1,$$

then we can obtain that

$$\frac{1}{2} g_2^1(z, 0, \mu) = \frac{1}{2} \text{Proj}_{\text{Ker}(M_2^1)} f_2^1(z, 0, \mu) = \begin{pmatrix} \mathcal{H}((B_{11}\mu_1 + B_{21}\mu_2) z_1) \\ (B_{13}\mu_1 + B_{23}\mu_2) z_3 \end{pmatrix},$$

where

$$\text{Ker}(M_2^1) = \text{span} \left\{ \begin{pmatrix} z_1 z_3 \\ 0 \\ 0 \end{pmatrix}, \begin{pmatrix} z_1 \mu_i \\ 0 \\ 0 \end{pmatrix}, \begin{pmatrix} 0 \\ z_2 z_3 \\ 0 \end{pmatrix}, \begin{pmatrix} 0 \\ z_2 \mu_i \\ 0 \end{pmatrix}, \begin{pmatrix} 0 \\ 0 \\ z_1 z_2 \end{pmatrix}, \begin{pmatrix} 0 \\ 0 \\ z_3^2 \end{pmatrix}, \begin{pmatrix} 0 \\ 0 \\ z_3 \mu_i \end{pmatrix}, \begin{pmatrix} 0 \\ 0 \\ \mu_1 \mu_2 \end{pmatrix}, \begin{pmatrix} 0 \\ 0 \\ \mu_i^2 \end{pmatrix} \right\}$$

with $i = 1, 2$. Moreover,

$$B_{11} = \eta_0^T L_1^{(1,0)} \xi_0, \quad B_{21} = \eta_0^T L_1^{(0,1)} \xi_0,$$

$$B_{13} = \eta_{k_*}^T \left(L_1^{(1,0)} \xi_{k_*} - \tilde{B} \xi_{k_*} \right), \quad B_{23} = \eta_{k_*}^T L_1^{(0,1)} \xi_{k_*}$$

with

$$\tilde{B} = \begin{pmatrix} -\frac{k_*^2}{\ell^2} & 0 \\ 0 & 0 \end{pmatrix}.$$

Next, by a slight modification of the calculation procedures in [34], we give the detail calculation procedures of $B_{11}, B_{21}, B_{13}, B_{23}, B_{210}, B_{102}, B_{111}, B_{003}$ steps by steps.

Step 1:

$$\begin{cases} B_{11} = \eta_0^T L_1^{(1,0)} \xi_0, & B_{21} = \eta_0^T L_1^{(0,1)} \xi_0, \\ B_{13} = \eta_{k_*}^T \left(L_1^{(1,0)} \xi_{k_*} - \tilde{B} \xi_{k_*} \right), \\ B_{23} = \eta_{k_*}^T L_1^{(0,1)} \xi_{k_*}, \\ B_{210} = C_{210} + \frac{3}{2} (D_{210} + E_{210}), \\ B_{102} = C_{102} + \frac{3}{2} (D_{102} + E_{102}), \\ B_{111} = C_{111} + \frac{3}{2} (D_{111} + E_{111}), \\ B_{003} = C_{003} + \frac{3}{2} (D_{003} + E_{003}). \end{cases}$$

Step 2:

$$\left\{ \begin{aligned} C_{210} &= \frac{1}{6\ell\pi} \eta_0^T A_{210}, & C_{102} &= \frac{1}{6\ell\pi} \eta_0^T A_{102}, \\ C_{111} &= \frac{1}{6\ell\pi} \eta_{k_*}^T A_{111}, & C_{003} &= \frac{1}{4\ell\pi} \eta_{k_*}^T A_{003}, \\ D_{210} &= \frac{1}{6\ell\pi\omega_c i} \left(-\left(\eta_0^T A_{200}\right) \left(\eta_0^T A_{110}\right) \right. \\ &\quad \left. + \left|\eta_0^T A_{110}\right|^2 + \frac{2}{3} \left|\eta_0^T A_{020}\right|^2 \right), \\ D_{102} &= \frac{1}{6\ell\pi\omega_c i} \left(-2 \left(\eta_0^T A_{200}\right) \left(\eta_0^T A_{002}\right) \right. \\ &\quad \left. + \left(\eta_0^T A_{110}\right) \left(\bar{\eta}_0^T A_{002}\right) + 2 \left(\eta_0^T A_{002}\right) \left(\eta_{k_*}^T A_{101}\right) \right), \\ D_{111} &= -\frac{1}{3\ell\pi\omega_c} \operatorname{Im} \left(\left(\eta_{k_*}^T A_{101}\right) \left(\eta_0^T A_{110}\right) \right), \\ D_{003} &= -\frac{1}{3\ell\pi\omega_c} \operatorname{Im} \left(\left(\eta_{k_*}^T A_{101}\right) \left(\eta_0^T A_{002}\right) \right) \end{aligned} \right.$$

with

$$\left\{ \begin{aligned} A_{200} &= \xi_{01}^2 f_{2000} + 2\xi_{01}\xi_{02} f_{1100} + \xi_{02}^2 f_{0200} = \bar{A}_{020}, \\ A_{002} &= \xi_{k_*1}^2 f_{2000} + 2\xi_{k_*1}\xi_{k_*2} f_{1100} + \xi_{k_*2}^2 f_{0200}, \\ A_{110} &= 2 \left(|\xi_{01}|^2 f_{2000} + 2 \operatorname{Re} \left(\xi_{01}\bar{\xi}_{02} \right) f_{1100} \right. \\ &\quad \left. + |\xi_{02}|^2 f_{0200} \right), \\ A_{101} &= 2 \left(\xi_{01}\xi_{k_*1} f_{2000} + \left(\xi_{01}\xi_{k_*2} + \xi_{02}\xi_{k_*1} \right) f_{1100} \right. \\ &\quad \left. + \xi_{02}\xi_{k_*2} f_{0200} \right) = \bar{A}_{011} \\ A_{210} &= 3 \left(f_{3000} |\xi_{01}|^2 \xi_{01} + f_{0300} |\xi_{02}|^2 \xi_{02} \right. \\ &\quad \left. + f_{2100} \left(\xi_{01}^2 \bar{\xi}_{02} + 2 |\xi_{01}|^2 \xi_{02} \right) \right. \\ &\quad \left. + f_{1200} \left(\xi_{02}^2 \bar{\xi}_{01} + 2 |\xi_{02}|^2 \xi_{01} \right) \right), \\ A_{102} &= 3 \left(f_{3000} \xi_{01} \xi_{k_*1}^2 + f_{0300} \xi_{02} \xi_{k_*2}^2 \right. \\ &\quad \left. + f_{2100} \left(\xi_{02} \xi_{k_*1}^2 + 2 \xi_{01} \xi_{k_*1} \xi_{k_*2} \right) \right. \\ &\quad \left. + f_{1200} \left(\xi_{01} \xi_{k_*2}^2 + 2 \xi_{02} \xi_{k_*1} \xi_{k_*2} \right) \right), \\ A_{111} &= 6 \left(f_{3000} |\xi_{01}|^2 \xi_{k_*1} + f_{0300} |\xi_{02}|^2 \xi_{k_*2} \right. \\ &\quad \left. + f_{2100} \left(|\xi_{01}|^2 \xi_{k_*2} + 2 \xi_{k_*1} \operatorname{Re} \left(\xi_{01}\bar{\xi}_{02} \right) \right) \right. \\ &\quad \left. + f_{1200} \left(|\xi_{02}|^2 \xi_{k_*1} + 2 \xi_{k_*2} \operatorname{Re} \left(\xi_{02}\bar{\xi}_{01} \right) \right) \right), \\ A_{003} &= \left(f_{3000} \xi_{k_*1}^3 + f_{0300} \xi_{k_*2}^3 \right) \\ &\quad + 3 \left(f_{2100} \xi_{k_*1}^2 \xi_{k_*2} + f_{1200} \xi_{k_*1} \xi_{k_*2}^2 \right). \end{aligned} \right.$$

Step 3:

$$\left\{ \begin{aligned} E_{210} &= \frac{1}{3\sqrt{\ell\pi}} \eta_0^T \left(\left(\xi_{01} f_{2000} + \xi_{02} f_{1100} \right) h_{0110}^{(1)} \right. \\ &\quad \left. + \left(\xi_{02} f_{0200} + \xi_{01} f_{1100} \right) h_{0110}^{(2)} \right. \\ &\quad \left. + \left(\bar{\xi}_{01} f_{2000} + \bar{\xi}_{02} f_{1100} \right) h_{0200}^{(1)} \right. \\ &\quad \left. + \left(\bar{\xi}_{02} f_{0200} + \bar{\xi}_{01} f_{1100} \right) h_{0200}^{(2)} \right), \\ E_{102} &= \frac{1}{3\sqrt{\ell\pi}} \eta_0^T \left(\left(\xi_{01} f_{2000} + \xi_{02} f_{1100} \right) h_{0002}^{(1)} \right. \\ &\quad \left. + \left(\xi_{02} f_{0200} + \xi_{01} f_{1100} \right) h_{0002}^{(2)} \right. \\ &\quad \left. + \left(\xi_{k_*1} f_{2000} + \xi_{k_*2} f_{1100} \right) h_{k_*101}^{(1)} \right. \\ &\quad \left. + \left(\xi_{k_*2} f_{0200} + \xi_{k_*1} f_{1100} \right) h_{k_*101}^{(2)} \right), \\ E_{111} &= \frac{1}{3\sqrt{\ell\pi}} \eta_{k_*}^T \left(\left(\xi_{01} f_{2000} + \xi_{02} f_{1100} \right) h_{k_*011}^{(1)} \right. \\ &\quad \left. + \left(\xi_{02} f_{0200} + \xi_{01} f_{1100} \right) h_{k_*011}^{(2)} \right. \\ &\quad \left. + \left(\bar{\xi}_{01} f_{2000} + \bar{\xi}_{02} f_{1100} \right) h_{k_*101}^{(1)} \right. \\ &\quad \left. + \left(\bar{\xi}_{02} f_{0200} + \bar{\xi}_{01} f_{1100} \right) h_{k_*101}^{(2)} \right) \\ &\quad + \eta_{k_*}^T \left(\left(\xi_{k_*1} f_{2000} + \xi_{k_*2} f_{1100} \right) \right. \\ &\quad \left. \left(\frac{1}{3\sqrt{\ell\pi}} h_{0110}^{(1)} + \frac{1}{3\sqrt{2\ell\pi}} h_{(2k_*)110}^{(1)} \right) \right. \\ &\quad \left. + \left(\xi_{k_*2} f_{0200} + \xi_{k_*1} f_{1100} \right) \right. \\ &\quad \left. \left(\frac{1}{3\sqrt{\ell\pi}} h_{0110}^{(2)} + \frac{1}{3\sqrt{2\ell\pi}} h_{(2k_*)110}^{(2)} \right) \right), \\ E_{003} &= \eta_{k_*}^T \left(\left(\xi_{k_*1} f_{2000} + \xi_{k_*2} f_{1100} \right) \right. \\ &\quad \left(\frac{1}{3\sqrt{\ell\pi}} h_{0002}^{(1)} + \frac{1}{3\sqrt{2\ell\pi}} h_{(2k_*)002}^{(1)} \right) \right. \\ &\quad \left. + \left(\xi_{k_*2} f_{0200} + \xi_{k_*1} f_{1100} \right) \right. \\ &\quad \left. \left(\frac{1}{3\sqrt{\ell\pi}} h_{0002}^{(2)} + \frac{1}{3\sqrt{2\ell\pi}} h_{(2k_*)002}^{(2)} \right) \right). \end{aligned} \right.$$

Here

$$f(U, \mu) = \sum_{i+j+l_1+l_2 \geq 2} \frac{1}{i!j!l_1!l_2!} f_{ijl_1l_2} u^i v^j \mu_1^{l_1} \mu_2^{l_2},$$

$$f_{ijl_1l_2} = \left(f_{ijl_1l_2}^{(1)}, f_{ijl_1l_2}^{(2)} \right)^T$$

with

$$f_{ijl_1l_2}^{(k)} = \frac{\partial^{i+j+l_1+l_2} F^{(k)}(0, 0, 0, 0)}{\partial u^i \partial v^j \partial \mu_1^{l_1} \partial \mu_2^{l_2}}, \quad k = 1, 2.$$

More precisely, for the system (29), by combining with Eq.(32), we have

$$\left\{ \begin{aligned} f_{2000} &= \left(\frac{-2\gamma + \frac{u_*v_*+4v_*h}{4\delta^*(u_*+h)^2\sqrt{u_*+h}}}{\frac{-u_*v_*-4v_*h}{4\delta^*(u_*+h)^2\sqrt{u_*+h}}} \right), \\ f_{1100} &= \left(\frac{-u_*-2h}{\frac{2\delta^*(u_*+h)\sqrt{u_*+h}}{u_*+2h}} \right), \quad f_{0200} = \begin{pmatrix} 0 \\ 0 \end{pmatrix}, \\ f_{3000} &= \left(\frac{\frac{-3u_*v_*-18v_*h}{8\delta^*(u_*+h)^3\sqrt{u_*+h}}}{\frac{3u_*v_*+18v_*h}{8\delta^*(u_*+h)^3\sqrt{u_*+h}}} \right), \quad f_{0300} = \begin{pmatrix} 0 \\ 0 \end{pmatrix}, \\ f_{2100} &= \left(\frac{\frac{u_*+4h}{4\delta^*(u_*+h)^2\sqrt{u_*+h}}}{\frac{-u_*-4h}{4\delta^*(u_*+h)^2\sqrt{u_*+h}}} \right), \quad f_{1200} = \begin{pmatrix} 0 \\ 0 \end{pmatrix}. \end{aligned} \right.$$

Furthermore, we have

$$\left\{ \begin{aligned} h_{0200} &= \frac{1}{\sqrt{\ell\pi}} (\mathcal{M}_0(2i\omega_c))^{-1} \\ &\quad \left(A_{200} - \left(\eta_0^T A_{200}\xi_0 + \bar{\eta}_0^T A_{200}\bar{\xi}_0 \right) \right), \\ h_{0020} &= \frac{1}{\sqrt{\ell\pi}} (\mathcal{M}_0(-2i\omega_c))^{-1} \\ &\quad \left(A_{020} - \left(\eta_0^T A_{020}\xi_0 + \bar{\eta}_0^T A_{020}\bar{\xi}_0 \right) \right), \\ h_{0002} &= \frac{1}{\sqrt{\ell\pi}} (\mathcal{M}_0(0))^{-1} \\ &\quad \left(A_{002} - \left(\eta_0^T A_{002}\xi_0 + \bar{\eta}_0^T A_{002}\bar{\xi}_0 \right) \right), \\ h_{0110} &= \frac{1}{\sqrt{\ell\pi}} (\mathcal{M}_0(0))^{-1} \\ &\quad \left(A_{110} - \left(\eta_0^T A_{110}\xi_0 + \bar{\eta}_0^T A_{110}\bar{\xi}_0 \right) \right), \\ h_{k_*101} &= \frac{1}{\sqrt{\ell\pi}} (\mathcal{M}_{k_*}(i\omega_c))^{-1} \left(A_{101} - \eta_{k_*}^T A_{101}\xi_{k_*} \right), \\ h_{k_*011} &= \frac{1}{\sqrt{\ell\pi}} (\mathcal{M}_{k_*}(-i\omega_c))^{-1} \left(A_{011} - \eta_{k_*}^T A_{011}\xi_{k_*} \right), \\ h_{(2k_*)002} &= \frac{1}{\sqrt{2\ell\pi}} (\mathcal{M}_{2k_*}(0))^{-1} A_{002}, \\ h_{(2k_*)110} &= (0, 0)^T. \end{aligned} \right.$$

References

1. Lotka, A.J.: Relation between birth rates and death rates. *Science* **26**(653), 21–26 (1907)
2. Volterra, V.: *Variazione e fluttuazioni del numero d'individui in specie animali conviventi*. Memorie della R. Acc. dei Lincei. **2**(6), 31–113 (1926)
3. Freedman, H.I.: *Deterministic Mathematical Models in Population Ecology*. Marcel Dekker, New York (1980)
4. Murray, J.D.: *Mathematical Biology I: An Introduction*, 3rd edn. Springer-Verlag, New York (2002)
5. Holling, C.S.: The components of predation as revealed by a study of small-mammal predation of the European pine sawfly. *Can. Entomol.* **91**(5), 293–320 (1959)

6. Aziz-alauoui, M.A., Okiye, M.D.: Boundedness and global stability for a predator–prey model with modified Leslie–Gower and Holling-type II type schemes. *Appl. Math. Lett.* **16**(7), 1069–1075 (2003)
7. Arditi, R., Ginzburg, L.R.: Coupling in predator–prey dynamics: ratio-dependence. *J. Theor. Biol.* **139**(3), 311–326 (1989)
8. Song, Y.L., Zou, X.F.: Spatiotemporal dynamics in a diffusive ratio-dependent predator–prey model near a Hopf–Turing bifurcation point. *Comput. Math. Appl.* **67**(10), 1978–1997 (2014)
9. Tripathi, J.P., Abbas, S., Thakur, M.: Dynamical analysis of a prey–predator model with Beddington–DeAngelis type function response incorporating a prey refuge. *Nonlinear Dyn.* **80**(1–2), 177–196 (2015)
10. Petrovskii, S., Morozov, A., Li, B.L.: Regimes of biological invasion in a predator–prey system with the Allee effect. *Bull. Math. Biol.* **67**(3), 637–661 (2005)
11. Wang, J.F., Shi, J.P., Wei, J.J.: Dynamics and pattern formation in a diffusive predator–prey system with strong Allee effect in prey. *J. Differ. Equ.* **251**(4–5), 1276–1304 (2011)
12. Peng, Y.A., Zhang, T.B.: Turing instability and pattern induced by cross-diffusion in a predator–prey system with Allee effect. *Appl. Math. Comput.* **275**, 1–12 (2016)
13. Ajraldi, V., Pittavino, M., Venturino, E.: Modeling herd behavior in population systems. *Nonlinear Anal. Real World Appl.* **12**(4), 2319–2338 (2011)
14. Saha, S., Samanta, G.P.: Analysis of a predator–prey model with herd behavior and disease in prey incorporating prey refuge. *Int. J. Biomath.* **12**(1), 1950007 (2019)
15. Manna, D., Maiti, A., Samanta, G.P.: Deterministic and stochastic analysis of a predator–prey model with Allee effect and herd behaviour. *Simulation* **95**(4), 339–349 (2019)
16. Maiti, A., Sen, P., Samanta, G.P.: Deterministic and stochastic analysis of a prey–predator model with herd behaviour in both. *Syst. Sci. Control Eng.* **4**(1), 259–269 (2016)
17. Murray, J.D.: *Mathematical Biology II: Spatial Models and Biomedical Applications*, 3rd edn. Springer-Verlag, Heidelberg (2003)
18. Du, Y.H., Shi, J.P.: A diffusive predator–prey model with a protection zone. *J. Differ. Equ.* **229**(1), 63–91 (2006)
19. Yi, F.Q., Wei, J.J., Shi, J.P.: Bifurcation and spatiotemporal patterns in a homogeneous diffusive predator–prey system. *J. Differ. Equ.* **246**(5), 1944–1977 (2009)
20. Cui, R.H., Shi, J.P., Wu, B.Y.: Strong Allee effect in a diffusive predator–prey system with a protection zone. *J. Differ. Equ.* **256**(1), 108–129 (2014)
21. Kerner, E.H.: A statistical mechanics of interacting biological species. *Bull. Math. Biol.* **19**(2), 121–146 (1957)
22. Shigesada, N., Kawasaki, K., Teramoto, E.: Spatial segregation of interacting species. *J. Theor. Biol.* **79**(1), 83–99 (1979)
23. Shukla, J.B., Verma, S.: Effects of convective and dispersive interactions on the stability of two species. *Bull. Math. Biol.* **43**(5), 593–610 (1981)
24. Tian, C.R., Lin, Z.G., Pedersen, M.: Instability induced by cross diffusion in reaction-diffusion systems. *Nonlinear Anal. Real World Appl.* **11**(2), 1036–1045 (2010)
25. Sun, G.Q., Jin, Z., Li, L., et al.: Spatial patterns of a predator–prey model with cross diffusion. *Nonlinear Dyn.* **69**(4), 1631–1638 (2012)

26. Guin, L.N.: Existence of spatial patterns in a predator–prey model with self- and cross-diffusion. *Appl. Math. Comput.* **226**(1), 320–335 (2014)
27. Zhang, J.Y., Yan, G.W.: Lattice Boltzmann simulation of pattern formation under cross-diffusion. *Comput. Math. Appl.* **69**(3), 157–169 (2015)
28. Gambino, G., Lombardo, M.C., Sammartino, M., et al.: Turing pattern formation in the Brusselator system with nonlinear diffusion. *Phys. Rev. E* **88**(4), 042925 (2013)
29. Berenstein, I., Beta, C.: Cross-diffusion in the two-variable Oregonator model. *Chaos Interdiscip. J. Nonlinear Sci.* **23**(3), 033119 (2013)
30. Fanelli, D., Cianci, C., Patti, F.D.: Turing instabilities in reaction–diffusion systems with cross diffusion. *Eur. Phys. J. B* **86**(4), 1–8 (2013)
31. Gambino, G., Lombardo, M.C., Sammartino, M.: Turing instability and pattern formation for the Lengyel–Epstein system with nonlinear diffusion. *Acta Applicandae Mathematicae* **132**(1), 283–294 (2014)
32. Tang, X.S., Song, Y.L., Zhang, T.H.: Turing–Hopf bifurcation analysis of a predator–prey model with herd behavior and cross-diffusion. *Nonlinear Dyn.* **86**(1), 1–17 (2016)
33. Faria, T.: Normal forms and Hopf bifurcation for partial differential equations with delay. *Trans. Am. Math. Soc.* **352**(5), 2217–2238 (2000)
34. Song, Y.L., Zhang, T.H., Peng, Y.H.: Turing–Hopf bifurcation in the reaction–diffusion equations and its applications. *Commun. Nonlinear Sci. Numer. Simul.* **33**, 229–258 (2016)
35. De Assis, R.A., Pazim, R., Malavazi, M.C., et al.: A mathematical model to describe the herd behaviour considering group defense. *Appl. Math. Nonlinear Sci.* **5**(1), 11–24 (2020)
36. Vitagliano, V.: Some phenomenological and thermodynamic aspects of diffusion in multicomponent systems. *Pure Appl. Chem.* **63**(10), 1441–1448 (1991)
37. Pao, C.V.: *Nonlinear Parabolic and Elliptic Equations*. Plenum Press, New York (1992)
38. Kuznetsov, Y.A.: *Elements of Applied Bifurcation Theory*, 3rd edn. Springer-Verlag, New York (2004)
39. Guckenheimer, J., Holmes, P.: *Nonlinear Oscillations, Dynamical Systems, and Bifurcations of Vector Fields*. Springer-Verlag, New York (1983)

Publisher’s Note Springer Nature remains neutral with regard to jurisdictional claims in published maps and institutional affiliations.